AUXILIARY-PATH-ASSISTED DIGITAL LINEARIZATION OF WIDEBAND WIRELESS RECEIVERS

A Thesis

by

LESTER BOAMPONG

Submitted to the Office of Graduate and Professional Studies of
Texas A&M University
in partial fulfillment of the requirements for the degree of

MASTER OF SCIENCE

Chair of Committee, Sebastian Hoyos
Committee Members, Edgar Sanchez-Sinencio
Javier A. Jo
Peng Li
Head of Department, Miroslave M. Begovic

May 2018

Major Subject: Electrical Engineering

ABSTRACT

Wireless communication systems in recent years have aimed at increasing data rates by ensuring flexible and efficient use of the radio spectrum. The dernier cri in this field has been in the area of carrier aggregation and cognitive radio. Carrier aggregation is a major component of LTE-Advanced. With carrier aggregation, a number of separate LTE carriers can be combined, by mobile network operators, to increase peak data rates and overall network capacity. Cognitive radios, on the other hand, allow efficient spectrum usage by locating and using spatially vacant spectral bands. High monolithic integration in these application fields can be achieved by employing receiver architectures such as the wideband direct conversion receiver topology. This is advantageous from the view point of cost, power consumption and size. However, many challenges exist, of particular importance is nonlinear distortion arising from analog front-end components such as low noise amplifiers (LNA). Nonlinear distortions especially become severe when several signals of varying amplitudes are received simultaneously. In such cases, nonlinear distortions stemming from strong signals may deteriorate the reception of the weaker signals, and also impair the receiver's spectrum sensing capabilities. Nonlinearity, usually a consequence of dynamic range limitation, degrades performance in wideband multi-operator communications systems, and it will have a notable role in future wireless communication system design.

This thesis presents a digital domain linearization technique that employs a very nonlinear auxiliary receiver path for nonlinear distortion cancellation. The proposed

linearization technique relies on one-time adaptively-determined linearization coefficients for cancelling nonlinear distortions. Specifically, we take a look at canceling the troublesome in-band third order intermodulation products using the proposed technique. The proposed technique can be extended to cancel out both even and higher order odd intermodulation products. Dynamic behavioral models are used to account for RF nonlinearities, including memory effects which cannot be ignored in the wideband scenario. Since the proposed linearization technique involves the use of two receiver paths, techniques for correcting phase delays between the two paths are also introduced. Simplicity is the hallmark of the proposed linearization technique. It can achieve up to +30 dBm in IIP3 performance with ADC resolution being a major performance bottleneck. It also shows strong tolerance to strong blocker nonlinearities.

DEDICATION

To my family and friends

ACKNOWLEDGEMENTS

My Heartfelt gratitude, first and foremost, goes to the Lord Jesus Christ for His superabundant grace and His ever-satisfying gift of righteousness. I am also grateful to my parents and siblings for their love, support and many prayers. I couldn't have come this far without you all.

I am exceedingly grateful to my advisor, Prof. Sebastian Hoyos, for his constant support, guidance and patience throughout my time at Texas A&M University. I couldn't have had a better supervisor. Thank you.

A big thank to all the pioneers of the Texas Instruments African Analog University Relations Program (TI-AAURP), especially Dee Hunter, Tuli Dake and Benjamin Sarpong. It was through their selfless pioneering work that my graduate education became a reality. Thank you all. It has been an exciting experience.

A big thank you to my colleague and friend, Patrick Kofi-Mensah Dollie (I had to mention all the names), for all your help and support. I could have made it without you. We have been more than study partners throughout our graduate studies.

Finally, I also want to extend my gratitude the PhD students I worked with on this project. I am also grateful to all the staff members of the Analog and Mixed Signal Center of Texas A&M University. Thank you all.

CONTRIBUTORS AND FUNDING SOURCES

This thesis work was supervised by a committee consisting of Dr. Sebastian Hoyos (Advisor), Dr. Edgar Sanchez-Sinencio, Dr. Peng Li of the Department of Electrical Engineering and Dr. Javier A. Jo of the Department of Biomedical Engineering.

All work in this thesis was completed by the student, in collaboration with Amir Tofighi Zavareh and Julian Gomez Diaz of the Department of Electrical Engineering.

Graduate study was supported by a fellowship from Texas A&M University funded by Texas Instrument Incorporated.

TABLE OF CONTENTS

Page

LIST OF FIGURES

Page

LIST OF TABLES

Page

1. INTRODUCTION

Wireless communication technology has become an integral part of our daily lives. This is evident from the everyday use of the cell phones, radios and other Wi-Fi-linked devices. This together with the growing trend towards cloud computing in recent years, and the push for internet of things has increased the need for high data rates. The demand for high data rates usually comes with the need for low cost, low-power-dissipating receivers. The traditional way of increasing data rates by using more bandwidth won't suffice as bandwidth is a resource that is rare. As such, we have turned to technique that allow flexible and efficient use of the available spectrum while increasing data rates. Some of these techniques include cognitive radio and carrier aggregation, to name but a few.

Carrier aggregation (CA) enables increase in peak data rates and overall network capacity. This is done by allowing users to download and upload data using a number of separate network carriers simultaneously. The separate carriers can be continuous or non-continuous inside the same band (intra-band CA), or from different bands (inter-band CA). CA allows exploitation of the current fragmented spectrum allocations. Cognitive radio (CR), however, allows efficient use of the available spectrum by automatically detecting and using temporarily vacant frequency channels [1], [2]. Software-defined radio, a transceiver that reconfigures its communication parameters to meet user and network demand, provide the necessary platform for CRs [3]. The current

trend towards these wideband techniques for increasing data rates is also driven by the high cost-efficiency and high integrability afforded by direct conversion receivers (DCRs). DCRs have been in the research domain since the 1980s and have become attractive in recent years.

There are several reasons for the recent attractiveness of direct conversion receivers. To begin with, they are easy to integrate compared with heterodyne receivers. Secondly, they are resilient to mismatch effects even better than image-reject receivers, and finally some of their earlier drawback which were due to the use of discrete transistors are resolved by monolithic integration [4]. DCRs are also driving multicarrier or multi-operator receivers in which signals from different operators and possibly different radio access networks are received at the same time using a single wideband receiver chain.

The multicarrier scenario puts strict requirements on the receiver components' linearity, especially the low noise amplifier (LNA), as the received multicarrier or multi-operator signals usually have different amplitude levels. Strong blockers received very close to the base-station may cause nonlinear distortions on weak signals received far away from the base station. The nonlinearity problem becomes particularly interesting in the case of CA and CR. Getting better linearity by using analog linearization techniques is challenging considering the usual limitations on power consumption, implementation cost and component count and PVT variations. However, digital signal processing (DSP) algorithms can be used to enhance the linearity of the received signal with added

advantages such as high robustness to PVT variations. This helps to relax the strict linearity requirement on the analog hardware and push the receiver performance beyond the current state-of-the-art receivers.

A lot of research work has been done on using DSP techniques in removing receiver nonidealities coming from the analog front-end. I/Q imbalance correction using DSP is a good example. A lot of research has been done on this issue [5]–[8]. While there has been some research done on suppressing distortion and interference due to nonlinearities in the receiver analog front-end, digital linearization of nonlinear distortions in the wideband multicarrier scenario has not receive much attention. This thesis takes a look into modeling and linearization of third order nonlinearities in wideband radio receivers. A new auxiliary-path-assisted digital linearization method based on background adaptively-determined linearization coefficients is proposed. This linearization method falls in the class of dual-path linearization techniques. In general, by using the proposed linearization technique, the tight linearity requirement on the analog front-end are relaxed. Moreover, this approach is more robust to process, voltage and temperature (PVT) variations as the linearization in done in the digital domain. Digital domain processing also renders this technique power-competitive due to CMOS process scaling, which is largely benefiting digital domain signal processing.

1.1 Organization

Since DCRs are driving cognitive radio and are preferable in carrier aggregated receiver, a detailed background of DCRs and the nonlinear distortions plaguing them is in order. This thesis is organized as follows; section 2 gives an overview of direct conversion receivers. LNA third order nonlinearity models are also looked at in this section. In section 3, existing auxiliary-path-assisted linearization techniques are also looked at. The proposed auxiliary-path-assisted linearization technique which uses DSP algorithms is presented in section 4. Simulation results are also presented in this section. Finally, in section 5, a summary and conclusion to this work is presented.

2 BACKGROUND

Wideband direct conversion receivers (DCRs) are preferred in modern wireless communication networks and radar systems because of their high component integrability, cost-effectiveness and flexibility [4], [9]. The basic idea behind DCRs is to down-convert the received signal directly to baseband or zero frequency as illustrated in Figure 2.1. In this way, the image signal becomes part of the received signal and problems associated with the image signal are avoided.

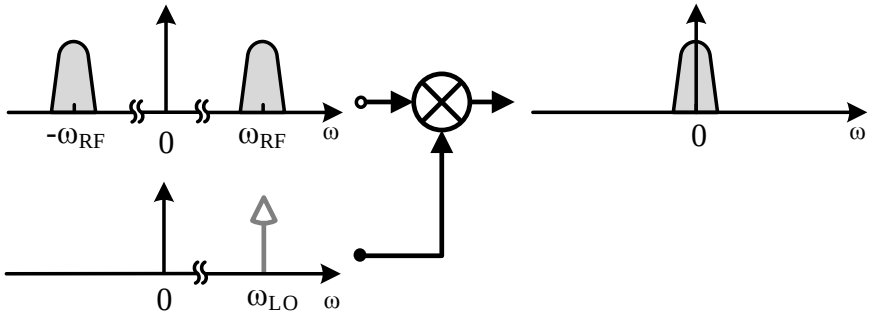

Figure 2.1: DCR scheme with respect to a single positive frequency

A widely used DCR is shown conceptually in Figure 2.2 below. In this Figure 2.2, the received signal is filtered (usually by using SAW filters), and then amplified using a low noise amplifier (LNA). The LNA should add little noise, and ideally no nonlinear distortion to the system, while providing sufficient signal power amplification. It should also be able to handle high interference levels in the received signal. The I/Q mixers are then used to down-convert the amplified signal directly from high frequency to baseband (zero frequency). I/Q channels are necessary in avoiding irreversible corruption in

phase-modulated and frequency-modulated signals. The two sidebands in these modulation schemes contain different information and must be separated into two phases to avoid overlap, and hence data corruption. The local oscillator (LO) provide stable signal for the mixer down-conversion process.

After down-conversion, low-pass filtering is done to suppress nearby interferers and also prevent aliasing in the analog to digital conversion process. A variable gain amplifier is sometimes employed, after the filtering, to provide optimum signal power for the baseband ADC. Next, analog to digital converters (ADCs) are used to digitize the lowpass-filtered signal. Digital post-processing such as channel equalization, channel selection and linearization of nonlinearities can then be done on the received signal. In order to make DCRs' integration easier, modern receiver chains totally remove the RF or SAW filter [10]–[14].

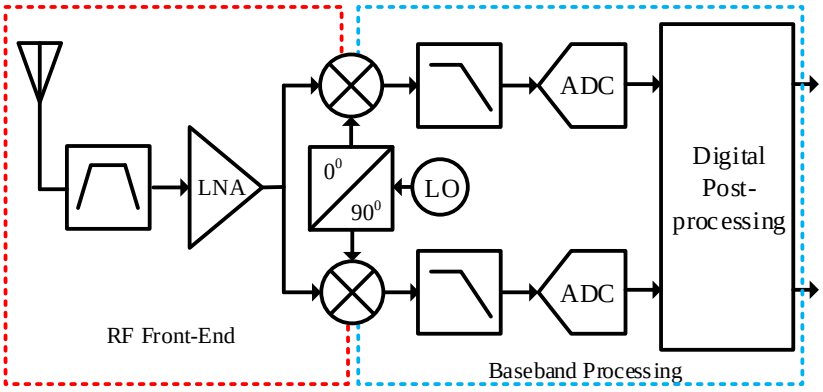

Figure 2.2: Direct Conversion Receiver

DCRs have several advantages over heterodyne receivers. First, the cancellation of the image frequency is no longer an issue because the intermediate frequency (IF) is zero. This eliminates the need for an image rejection filter which also means that the LNA does not have to drive a 50Ω load [4]. Also, CDRs do not require an IF filter. They only require low-pass filters which are easy to integrate monolithically. DCRs do come with some implementation issues which makes their system performance poor. But with the current advancement in DSP techniques for mitigating these issues, a lower performance can be accepted as a trade-off with high on-chip integration that DCRs offer. Some of the design implementation issues as well as dynamic range requirement are discussed here briefly with special focus on linearity which is the theme of this thesis.

2.1 DCR Design Issues

2.1.1 DC offset

Since in DCRs the signal is down-converted to zero IF, unwanted DC offset can corrupt the signal and also saturate subsequent stages. Mixer mismatches and self-mixing of the LO signal are usually the cause of DC offsets [4], [15], [16]. Mismatch between mixer components produce a constant DC offset while self-mixing generates a time-varying DC offset [17].

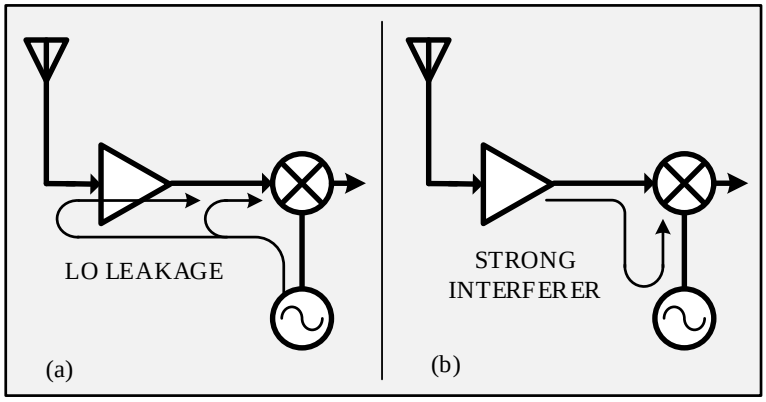

Figure 2.3: Leakages in the local oscillator

As illustrated in Figure 2.3, there exist some leakage in the mixer because of poor isolation between the RF and LO ports. The LO radiation can reach the LNA and propagate through the front-end. Likewise, the RF signal can also reach the LO input of the mixer. These signals cause self-mixing that generates high DC offset at the mixer output. Immediately following the mixer are a chain of directly coupled high-gain components that can boost any amount of DC offset and saturate subsequent blocks.

AC coupling at the output of the mixer can be used as a possible solution to the problem of DC offset but they corrupt the down-converted signals. Therefore, offset cancellation techniques are needed to make DCRs useable. Modulation schemes that are "DC-free" like binary frequency shift keying (BPSK) can also be employed [4], [17]. But their spectral efficiency is poor compared with other digital modulation schemes; something that should also be considered.

2.1.2 Flicker noise

Noise in the receiver can be evaluated in two distinctive ways, viz., the additive noise expressed by noise figure and the low-frequency flicker noise of the baseband components [18]. In DCR converters, the low-frequency flicker noise becomes a profound in-band phenomenon that needs to be considered as the received signal is directly down-converted to baseband. This is illustrated in Figure 2.4.

Flicker noise effects can be minimized by combining different techniques. First of all, the number of baseband active devices can be reduced. This reduces the flicker noise contribution of each individual transistor. Secondly, the front-end circuitries can also be designed with sufficient gain to reduce the effects of flicker noise. Larger transistor devices can also be used to reduce flicker noise amplitude since the stages after the mixer operate at low frequency. Certain technology processes are also known to have low flicker noise.

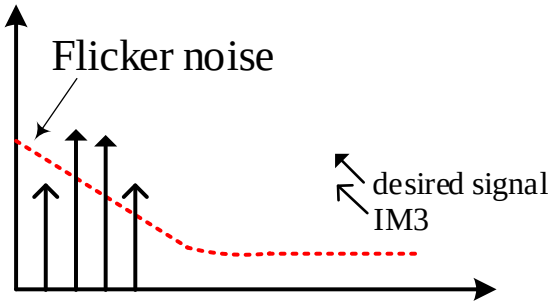

Figure 2.4: Down-converted signal and flicker noise

2.1.3 Intermodulation

Wideband receivers, especially DCRs, which have little analog selectivity, tend to be susceptible to intermodulation effects – a consequence of the nonlinearities in the receiver components. Intermodulation leads to the creation of extra unwanted signal components which distort the received signal. It is mostly produced by nonidealities in the LNA and the mixer. Not only are DCRs susceptible to odd-order intermodulation but they are also susceptible to even-order intermodulation. It has been shown in [19] and [20] that balanced topologies are effective in minimizing DC offsets and even-order intermodulation. Even-harmonic mixing, introduced in these papers is also a promising alternative. Other methods with special focus on digital techniques for minimizing even-order intermodulation have also been proposed in literature [21]–[24].

Traditionally, intermodulation products that fall outside the band of interest were simply be filtered out, and those falling in the band of interest, a well-known example being the third order intermodulation product, required a more sophisticated cancellation technique. However, in the case of carrier aggregation, especially in the case of continuous intra-band carrier aggregation, both types of intermodulation require sophisticated cancellation techniques as separate bands spanning a wide portion of the spectrum are being aggregated together. Intermodulation products that fall outside the "band of interest" may technically fall in another band that is part of the carrier components to be aggregated.

2.2 Dynamic Range Requirement

Spectrum usage efficiency can be improved by using spectrum sensing and dynamic spectrum access. In simple terms, spectrum sensing involves measuring the energy in a particular frequency band and comparing it to a predetermined noise level in order to determine whether it is occupied or not, and dynamic spectrum access is the means of exploiting vacant frequency bands. Both techniques are essential to cognitive radios implementation.

Dynamic range of a receiver is the span of signal amplitudes over which the receiver can operate. The lower boundary of this range is determined by the noise floor, and its upper boundary is governed by its strong-signal-handling capability. Limited receiver dynamic range impairs spectrum sensing algorithms and dynamic spectrum access in many ways as it puts a constraint on the linearity of the receiver. Figure 2.5 is used as an example to illustrate the impairment caused by limited dynamic range. A wideband multicarrier receiver simultaneously receives both weak and strong signals through a single receiver chain. As a result of limited receiver dynamic range, the strong signals in bands 2 and 4 cause nonlinear distortion on the weak signal in band 3 which deteriorates the weak signal. In reality, the amplitude range in the received signal can be tens of dBs, and as such requires large dynamic range from the receiver. UTMS for example requires at least 70dB SFDR [25].

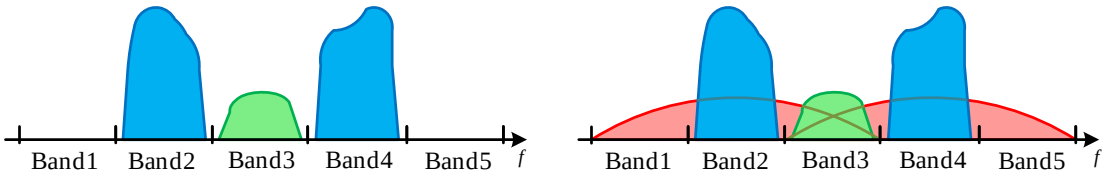

(a) Ideal linear receiver (b) Nonlinear receiver

Figure 2.5: Illustration of dynamic range limitation

In the case of spectrum sensing, sensing bands 2,3 and 4 in the nonlinear receiver would give the information that these bands are occupied, which is true. However, sensing bands 1 and 5 would give the information that these bands are also occupied due to the energies (from nonlinear components) present in these bands. This is a false alarm which would prevent a cognitive radio system from hopping into these band. The energies present in bands 1 and 5 are as a result of the nonlinear distortion resulting from limited dynamic range in the receiver. In the case of carrier aggregation, this might mean a harmonic distortion stemming from an uplink band falling into a downlink band.

Although the noise floor (which determines the sensitivity of the receiver) is important, receiver's ability to handle strong signals is also very important. If the dynamic range is limited, not by the noise floor, but by its ability to handle strong signals, strong signals would generate harmonics and intermodulation products in the receiver. The latter being a problem that needs looking into. We take a look at the third order intermodulation product (IM3) generated by the LNA and how it can be removed.

2.3 RF Nonlinearities

RF nonlinearities comprise mostly of nonlinearities originating from the low noise amplifier (LNA) in DCRs. Mixers also do contribute their quota to the RF nonlinearities. These nonlinearities include harmonics and intermodulation products.

Ideally, one would expect a linear relationship between the low noise amplifier's input and output but because of limited headroom or dynamic range, it gets saturated by strong signals. This rather creates a nonlinear relationship between its input and output. The nonlinear input-output relationship produces nonlinear distortion i.e. additional unwanted frequency components including the troublesome third order intermodulation product. Due to the wide variations in the amplitude of received signals in wideband multicarrier receivers it is impossible to curb distortions due to these nonlinearities without increasing power consumption [26], [27].

Nonlinear systems are usually characterized by using a single tone signal or a multi-tone signal. If a single tone signal with frequency f is used, the output will have additional frequency components at nf, where n is a non-zero positive integer. The additional frequency components are the *harmonics*.

A two-tone signal with frequencies f_1 and f_2 would produce frequency components at $mf_1 \pm nf_2$ as well as harmonics of the individual fundamental frequencies (nf_1 and nf_2). m and n are positive non-zero integers. The new frequency components at $mf_1 \pm nf_2$ are the *intermodulation products*. The most troublesome intermodulation product is the third

order intermodulation product (IM3). It most often than not falls into the frequency band of interest which makes it difficult to filter out. The order of the intermodulation products is defined by $|m| + |n|$. For the IM3, $|m| + |n| = 3$, which means that $|m|$ and $|n| \in \{1,2\}$ but $|m| \neq |n|$.

The third order intercept point (*IIP3 or OIP3*) is used to characterize the IM3 product. The concept of IIP3 or OIP3 is depicted in Figure 2.6. IIP3 is the fictitious point on the Pi (x-axis) where the ideal linear and ideal third order gains intersect. OIP3 is the trace on the Po (y-axis) where this intersection point occurs. The higher these parameters are the more linear the system is. The linear gain has a slope of 1, and the third order gain has a slope of 3. Another important point on Figure 2.6 is the 1dB compression point. It is the point where the difference between the device's actual output and the linear output is exactly 1dB.

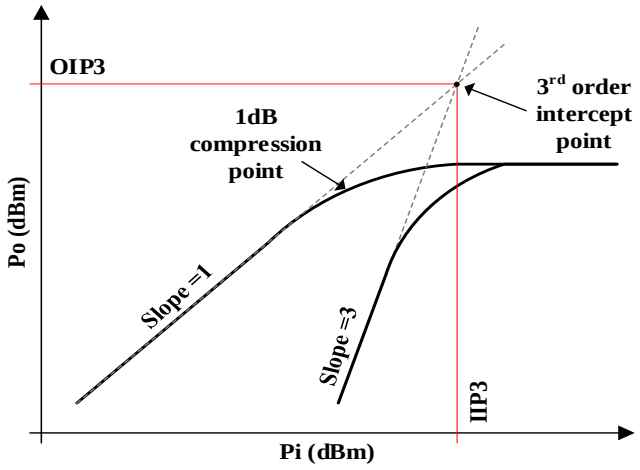

Figure 2.6: Third order intercept point

2.4 Modeling RF Nonlinearities

Modeling refers to the act of using mathematical equations to represent real-world objects and phenomena. Modeling can be classified into two, namely, physical modeling and behavioral modeling.

2.4.1 Physical modeling

Physical models are models that rely on knowledge of the individual components that make up the real-world object. The knowledge required to do this modeling include the constitutive relations of the individual components and the theoretical rules describing their interactions [28]. These models are appropriate for circuit-level simulation and provide accurate results at the expense of high simulation time.

2.4.2 Behavioral modeling

Models that require no a priori knowledge of the constituents of the system to be modelled are referred to as behavioral models. They are also referred to as black-box models. They rely on carefully selected input-output observations, and parameters extracted from such observations. Their accuracy is sensitive to the parameter extraction procedure used and the quality of the set of inputs used for the parameter extraction [28]. These models are used to model the RF nonlinearities in this work. As was stated before,

RF nonlinearities are mostly due to LNA nonlinearities. Hence, we take a look at LNA behavioral modelling. The inherent limitations of behavioral models are also taken into consideration here.

2.5 LNA Behavioral Modeling

Electronic devices are inherently nonlinear, and the LNA is no exception. Nonlinearity is not desirable for an LNA. A nonlinear LNA can be modeled using a memoryless or static behavioral model shown in (*1*) where *x(n)* is the input, and *y(n)* is the output. With static models, the current output of the system to be modelled is assumed to be a nonlinear function of the current inputs only, and previous inputs have no effect on the current output. These models only consider amplitude-amplitude conversions, and assume that the amplifier has a constant gain within its pass-band. They are fairly accurate for narrow-band frequency spectrums.

$$y(n) = \sum_{k=1}^{K} a_k x(n)^k = a_1 x(n) + a_2 x(n)^2 + a_3 x(n)^3 + \cdots \qquad (1)$$

For a two-tone input, the "tones" being at frequencies w_1 and w_2, the output of the nonlinear system modelled by the first three terms in (*1*) will be given by:

$$
\begin{aligned}
y(t) = & \frac{a_2}{2} \\
& + \left(a_1 + \frac{9a_3}{4}\right) cos(\omega_1 t) + \left(a_1 + \frac{9a_3}{4}\right) cos(\omega_2 t) \\
& + \frac{a_2}{2} cos(2\omega_1 t) + \frac{a_2}{2} cos(2\omega_2 t) \\
& + a_2 cos(\omega_1 - \omega_2)t + a_2 cos(\omega_1 + \omega_2)t \\
& + \frac{a_3}{4} cos(3\omega_1 t) + \frac{a_3}{4} cos(3\omega_2 t) \\
& + \frac{3a_3}{4} cos(2\omega_1 + \omega_2)t + \frac{3a_3}{4} cos(2\omega_2 + \omega_1)t \\
& + \frac{3a_3}{4} cos(2\omega_1 - \omega_2)t + \frac{3a_3}{4} cos(2\omega_2 - \omega_1)t
\end{aligned} \tag{2}
$$

The first line is a DC term, and the second line of terms is the fundamental frequency signals with third order gain compression. In the next line are the second order harmonics. The fourth line contains the second order intermodulation terms, and the fifth line contains the third order harmonics. The sixth and seventh lines contain the third order intermodulation distortion terms. The 3rd order intermodulation terms found in seventh line are the most troublesome as they mostly fall near the fundamental components. The newly generated spurious frequency components – harmonics and intermodulation products alike – are as a result nonlinearity. Same phenomenon happens in the nonlinear LNA. The model used in (*1*) is but a memoryless one, and is not enough to fully represent the nonlinearities in the LNA, especially in the wideband scenario. We now consider dynamic models for such nonlinear systems.

The reality is, most system are dynamic nature; their current output depends on their current inputs as well as their past inputs. This is known as memory or dynamic effect, and it is as a result of physical phenomena such as long time constants in DC bias circuits, bias modulation, trapping effects, and thermal effects due to self-heating [29]. Memory effects can be seen as the time-domain view of frequency dependence [30]. In simple terms, it accounts for the change in the gain and phase of a system as function of frequency. It can be seen as the asymmetries in the amplitudes of upper and lower sidebands, and frequency dependent asymmetries in the amplitude of intermodulation products. Figure 2.7 shows the frequency characteristics of the LNA, HD24089 [31], used in [32]. The frequency characteristic in this figure clearly shows the non-constant, frequency-dependent gain due to memory effects. Memory effects become severe in higher bandwidth applications such as WCDMA [33] and carrier aggregation, and as such models that consider memory effects are used this work.

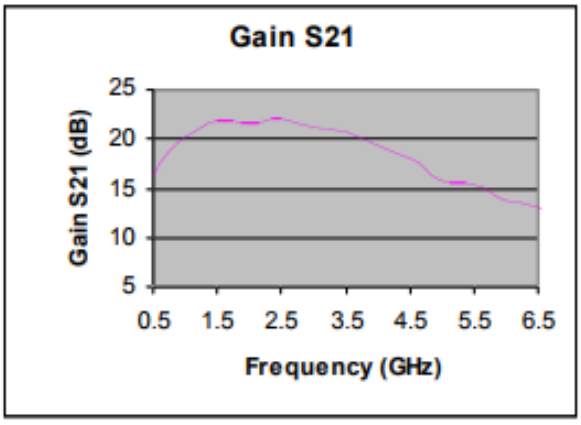

Figure 2.7: HD24089 Low noise amplifier frequency response. Reprinted from [31]

In general, a nonlinear system with memory effects can be modelled behaviorally using Volterra series which can be seen a Taylor series with memory [26],[27]. However, there is an exponential increase in the number of parameters as the memory length and the order of the nonlinearity increase. This renders the use of the Volterra series highly unrealistic. Special cases of the Volterra series such as the Hammerstein model and the Wiener model can be used to denote nonlinear systems with memory effects. The Wiener model is made up of a linear filter or linear time invariant system followed by a memoryless nonlinearity. The Hammerstein model has the reversed order of the two blocks i.e. it is made up of a static nonlinearity followed by a linear filter or a linear time invariant (LTI) system. The Hammerstein model is utilized in this thesis work.

The Hammerstein model is illustrated in Figure 2.8. It consists of a memoryless nonlinearity and a linear dynamic system.

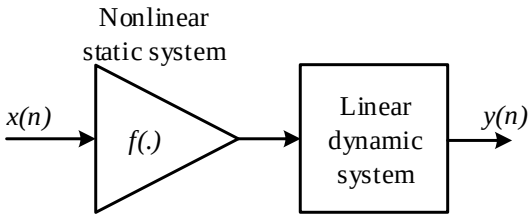

Figure 2.8: Hammerstein model

This model is expressed mathematically as shown in (*2*) [34], [35] where *Q* is the memory depth, *K* is the order of the nonlinearity polynomial, a_k are the polynomial

coefficients of the nonlinearity and *H(q)* is the filter transfer function for the K^{th} polynomial contribution.

$$y(n) = \sum_{k=1}^{K} \sum_{q=0}^{Q} a_k h(q) x^k (n-q) \tag{3}$$

The model in (*3*) can be simplified by using a variation of the Hammerstein model known as the parallel Hammerstein model. This variation of the Hammerstein model considers only the odd-order terms of the nonlinearity polynomial. The use of this model is fairly justified as the even-order nonlinearities most often than not fall outside the band of interest and can easily be filtered out. Furthermore, using differential circuits minimizes the effects of even-order nonlinearities. The parallel-Hammerstein model is expressed mathematically as in (*4*) where $a_{2k-1,q}$ corresponds to the impulse responses that model memory effect for each nonlinear coefficient.

$$y(n) = \sum_{q=0}^{Q} \sum_{k=1}^{K} a_{2k-1,q} x^{2k-1} (n-q) \tag{4}$$

Amongst the odd-order nonlinearities present in (*4*), the third order nonlinearity is the strongest in typical RF front-ends. The higher odd-order nonlinearities tend to fall below the noise floor of the receiver [3]. Hence, *K* in (*4*) is limited to 2. Equation (*4*), now becomes

$$y(n) = \sum_{q=0}^{Q} \sum_{k=1}^{2} a_{2k-1,q} x^{2k-1}(n-q) \tag{5}$$

$$y(n) = \sum_{q=0}^{Q} a_{1,q} x(n-q) + \sum_{q=0}^{Q} a_{3,q} x^{3}(n-q) \tag{6}$$

$$\begin{aligned} y(n) = {} & a_{1,0} x(n) + a_{3,0} x^{3}(n) \\ & + a_{1,1} x(n-1) + a_{3,1} x^{3}(n-1) \\ & + a_{1,2} x(n-2) + a_{3,2} x^{3}(n-2) \\ & + a_{1,3} x(n-3) + a_{3,3} x^{3}(n-3) + \cdots \end{aligned} \tag{7}$$

The first line in (*7*) is for the case of static/memoryless nonlinearity it can be seen as (*1*) without the even-order nonlinearity, and of course, the odd-order nonlinearity limited to the first and third orders only. For simplicity and ease of analysis and understanding, the nonlinear model will be limited to the first line in (*7*), and it is repeated in (*8*) as a separate equation for convenience. The reader must know that the full parallel-Hammerstein model is used in modeling the LNA for testing the proposed linearization technique.

$$y(n) = a_{1,0} x(n) + a_{3,0} x^{3}(n) \tag{8}$$

Equation (*8*) represents memoryless nonlinearity, and henceforth, the subscript "*0*" will be omitted. It is used for ease of analysis, and analysis will be extended to include memory effects wherever necessary. Coefficients a_1 and a_3 represent the linear gain and

third order distortion level respectively. These coefficients are related to the amplitude of IIP3 by the following expression:

$$A_{IIP3} = \sqrt{\frac{4|a_1|}{3|a_3|}} \tag{9}$$

3 AUXILIARY-PATH-ASSISTED LINEARIZATION SOLUTIONS

The performance of a receiver system is determined largely by the quality of its front-end circuits such as the LNA which processes all the interference and noise from the wireless channel. The challenge in LNA design is meeting its gain, noise, linearity and power consumption requirements simultaneously. Poor linearity leads to nonlinear distortions. In the case of wideband receivers, multiple channels are received simultaneously without filtering and they act as in-band interferers. As such, LNAs used in wideband receivers must have high linearity across very wide frequency ranges.

A good way to avoid nonlinear distortion, is to avoid the generation of the distortion in the first place. But due to the aforementioned trade-offs such as the gain-linearity trade-off, it is practically impossible to avoid nonlinear distortion, and as such techniques for cancelling it have to be developed. The nature of the problem is such that it yields a plausible solution, and these solutions have to be exploited. We take a look at linearization techniques that employ auxiliary receiver paths in mitigating nonlinearity especially odd-order nonlinearity. We categorize these linearization techniques into analog techniques, and digital techniques. Digital linearization techniques are preferred to analog techniques because of their robustness to PVT variations.

3.1 Analog Auxiliary-Path-Assisted Linearization Techniques

Many analog design techniques aimed at improving the IIP3 of the LNA and hence that of the receiver have been proposed in literature. Generally, LNA linearization is a challenging problem that calls for innovative techniques as solution. Traditional LNA linearization techniques such resistive source degeneration, on one hand, cannot suffice as they lead to gain degradation. Inductive source degeneration, on the other hand, suffers IIP3 degradation due to second-order interactions. CMOS transistors, which are intrinsically linear compared with bipolar transistor, can offer some linearity improvement but they require high DC current to give the needed linearity. These are some indicators of the need for sophisticated techniques such as dual receiver/LNA path techniques in dealing with nonlinearity.

Generally, LNA nonlinearities stem from two primary sources [36]:

1. Nonlinear transconductance g_m: translates input voltages to nonlinear output currents
2. Nonlinear output conductance g_{ds}: prominent when output voltage swings are high, and also when operating in the triode region (small V_{ds}); also known as output limited.

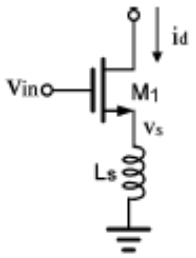

Figure 3.1: LNA with inductive source degeneration

For the simple inductively source degenerated LNA shown in Figure 3.1, the nonlinear output current can be expressed, in line with (*1*), as:

$$i_d = g_1(v_{in} - v_s) + g_2(v_{in} - v_s)^2 + g_3(v_{in} - v_s)^3 \tag{10}$$

The i^{th} order nonlinear coefficient can be obtained by differentiating I_{ds} with respect to V_{gs} at the bias point.

$$g_1 = \frac{\partial I_{ds}}{\partial V_{gs}}, \quad g_2 = \frac{1}{2!}\frac{\partial^2 I_{ds}}{\partial V_{gs}^2}, \quad g_1 = \frac{1}{3!}\frac{\partial^3 I_{ds}}{\partial V_{gs}^3} \tag{11}$$

A negative feedback system with linear feedback factor can be used to improve the linearity of the nonlinear amplifier. However, linearity enhancement using feedback isn't effective in LNAs due to low open loop gain and second-order interactions. The latter can be mitigated by using harmonic termination [36]–[38]. Next, we discuss some analog auxiliary-path-assisted linearization techniques.

In [39], an auxiliary signal path with signal scaling factors, *b* and $1/b^n$, and an amplifier well-matching the main path amplifier is used in linearizing the main LNA as

shown in Figure 3.2. The auxiliary path is used to reproduce the nonlinearities in the main path. The value of *n* determined by the order of the intermodulation product to be cancelled; *n = 2* for second order and *n = 3* for third order.

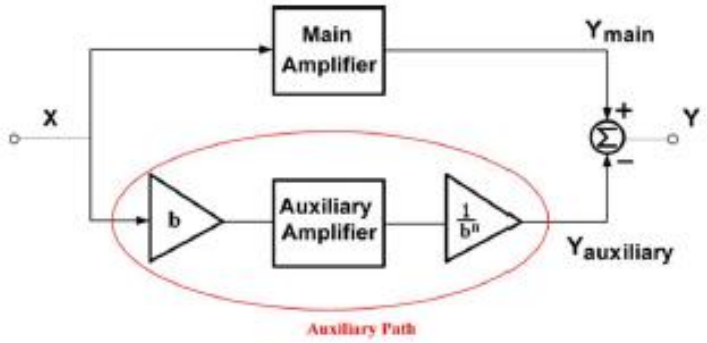

Figure 3.2: The feedforward linearization technique. Reprinted from [36]

The auxiliary path's output is subtracted from the main path's output for distortion cancellation. The concept is demonstrated mathematically in (*12*) in which case the third order nonlinearity is being cancelled.

$$
\begin{aligned}
Y_{main}(x) &= Ax + a_2Ax^3 \\
Y_{aux}(bx) &= Abx + a_2b^3Ax^3 \\
Y &= Y_{main}(x) - \frac{1}{b^3}Y_{aux}(bx) \\
Y &= A\left(1 - \frac{1}{b^2}\right)x
\end{aligned}
\tag{12}
$$

In general, the output is given by (*13*):

$$Y = A\left(1 - \frac{1}{b^{n-1}}\right)x \tag{13}$$

A major drawback of this approach is that it heavily relies on the auxiliary amplifier being a precise replica of the main amplifier, and would suffer in the presence of mismatches. Also, as seen from (*13*), the linear suffers attenuation by a factor of $(1 - 1/b^{n-1})$. [36] talks about gain boosting techniques by rearranging the scaling factors. It also introduces a way to cancel both second order and third order intermodulation terms concurrently.

In [40]–[45], the "conventional" derivative superposition (DS) method is introduced. This technique is so called because it sums the third derivative (g_3) of the auxiliary and main path transistors' drain currents in order to cancel out IM3. One implementation of this method is shown in Figure 3.3a. The IM3 cancellation for this implementation is shown in Figure 3.3b. This implementation relies on the fact that the sign of g_3 changes at the transition between weak and moderate inversion. Consequently, with appropriate biasing, the leftover g_3 becomes zero, and linearity is increased but only within a limited bias voltage range. In comparison with the optimum biasing [46] approach, this approach is much less susceptible to PVT variations. It also consumes less power as the auxiliary transistor operates in the weak-inversion region. A major drawback of this approach is that g_3 is only cancelled within a narrow bias voltage range, and would require extra auxiliary transistors to widen the bias voltage range.

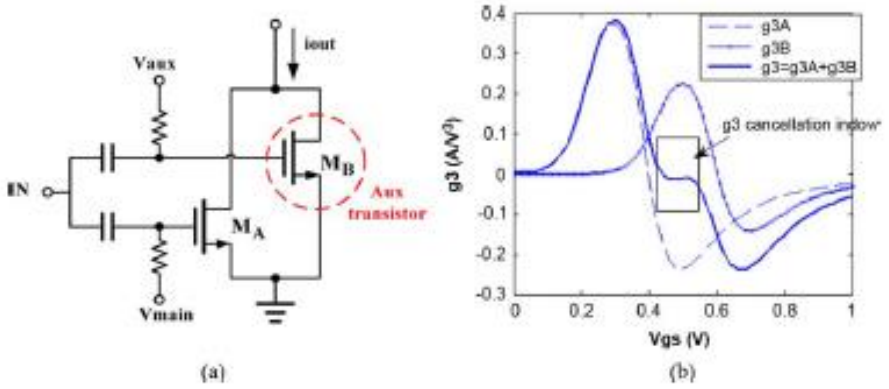

Figure 3.3: a) Dual-NMOS DS method b) Linearization mechanism. Reprinted from [36]

Several variations of the derivative superposition method also exist in literature; each aimed at improving the performance of the conventional DS scheme. Some of these variations are discussed in [36] and [47]. In [48], the complementary DS is introduced. It uses the complementary nature of PMOS and NMOS to help mitigate IM3 as well as IM2 since IM2 cancellation is not addressed by the conventional DS method. But there is tradeoff between IM3 cancellation and IM2 cancellation. [49] and [50] also looks at solving the IM3 problem along with IM2 cancellation. [51]–[53] introduce the modified DS which aims at total IM3 cancellation by tackling IM3 produced by second order interactions (not considered by the conventional DS) in the LNA. [54] aims at increasing the bias voltage range for a PVT-variation-robust g_3 cancellation. [55] tackles the low input impedance which leads to gain degradation in the conventional DS.

In [56], the second order intermodulation (IM2) injection technique is introduced. This technique eliminates the need for an explicit auxiliary path and it is particularly useful for differential transconductances. It exploits the second order nonlinearity of the device to be linearized.

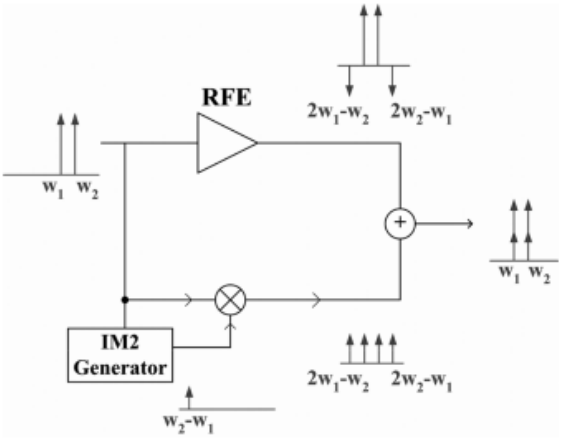

Figure 3.4: Concept of the IM2 injection method. Reprinted from [56]

A block diagram depicting this technique is shown in Figure 3.4. In this method, an IM2 product with low frequency is injected into the circuit to be linearized. The injected IM2 product is phase inverted and mixed with the input signal to produce the IM3 products for cancellation. This method relies on second-order interactions to cancel out IM3 products. Optimum results are obtained by injecting low-frequency IM2 signals. Some of the drawbacks of this technique include the fact that other injected IM2 products that are not low-frequency deteriorates performance. Also, the spacing of the two tones used in generating the IM2 products significantly affects performance.

3.2 Digital Auxiliary-Path-Assisted Linearization Techniques

Advanced DSP techniques have many important applications in receiver signal processing. One of the most interesting uses of DSP techniques is the possibility of improving the receiver's linearity performance by mitigating nonlinear effects caused by the receiver front-end components. A well-known example is in the area of I/Q mismatches and their correction using DSP techniques. It also well known that while the downscaling of CMOS processes and the constant reduction in supply power worsen noise and linearity in analog circuits, they largely benefit DSP systems from the view point of robustness, power consumption and processing speed. This trend is making DSP based linearization techniques more and more attractive in comparison with analog based techniques. Both single receiver path and dual receiver path DSP-based linearization techniques have been proposed in literature. We take a look at some of the auxiliary receiver path assisted DSP-based linearization techniques proposed in literature. These methods fall into the category of dual receiver path linearization techniques.

In [10] and [57], a digital domain linearization technique is introduced which is shown conceptually in Figure 3.5. In this work, a cubic term generator is used in an alternate path to generate reference IM3 products at RF. With the alternate path's LO frequency tuned to be the same as main path's LO frequency, the right group of third order intermodulation products are down-converted. Filtering of the baseband signal is

also done to attenuate unwanted IM products. The down-converted alternate-path IM3 products are equalized in the digital domain by means of adaptive filters to be the same as the IM3 products distorting the main path signal, and simple subtraction is done in the digital domain to cancel out IM3 products from the main path. The implemented receiver architecture is also shown in Figure 3.6.

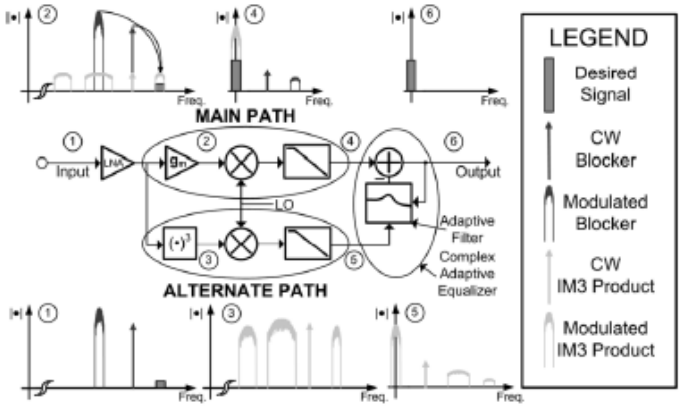

Figure 3.5: Feedforward error cancellation concept. Reprinted from [10]

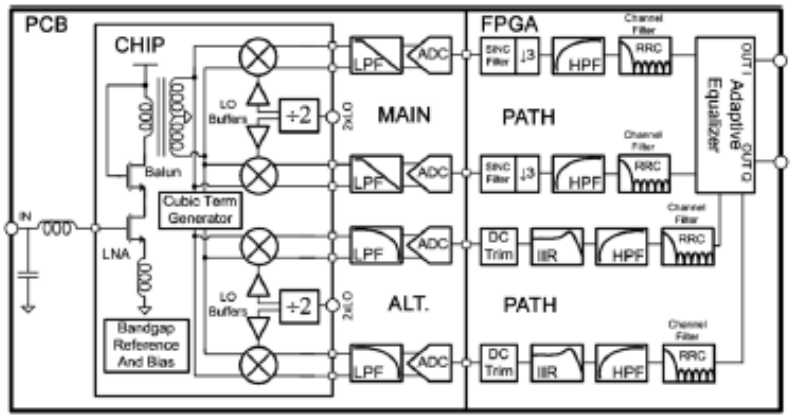

Figure 3.6: Experimental receiver architecture. Reprinted from [10]

A similar approach is proposed in [58] and [59] in which case an analog square term generator is also incorporated in addition to the cubic term generator, to produce even-order and higher odd-order intermodulation terms for further linearity improvement. A major disadvantage of these approaches is that they require specific analog receiver hardware, and analog squaring and cubing functions which are mostly inaccurate introduce extra nonlinear components. If the extra nonlinear terms as well as the linear feedthrough term are not properly attenuated, the digital adaptive filters may never converge, and if they do, they would incur high convergence time and their final values would be inaccurate.

In [32], two digital linearization techniques are introduced, namely, the reference-receiver-enhanced adaptive interference cancellation (RR-AIC) and the reference-receiver-aided nonlinearity inversion (RR-INV). The reference-receiver-enhanced adaptive interference cancellation (RR-AIC) is shown in Figure 3.7. In the RR-AIC approach, a reference receiver chain in which the RF LNA is removed is used. The LNA is removed so that a more linear signal without any RF nonlinear distortion would be obtained. Furthermore, I/Q correction is done in the digital domain with the aim of making the signal on the reference path distortion-free thereby improving the quality of the reference signal. Nonlinear models based on the parallel Hammerstein model are used, in the digital domain, to generate nonlinear components from the linear auxiliary reference signal. Next, parallel adaptive filters are used to equalize the generated

nonlinear components which yield an overall estimate of the nonlinearities present in the main receiver path. In this way, simple subtraction of the combined equalized auxiliary path nonlinear components from the main path signal yields a linear received signal. A disadvantage of this technique is that the models used to generate the nonlinear components are hardware specific and the calibration performance is limited by the models used. Also, the number of adaptive filters grow as the number of nonlinear components increase.

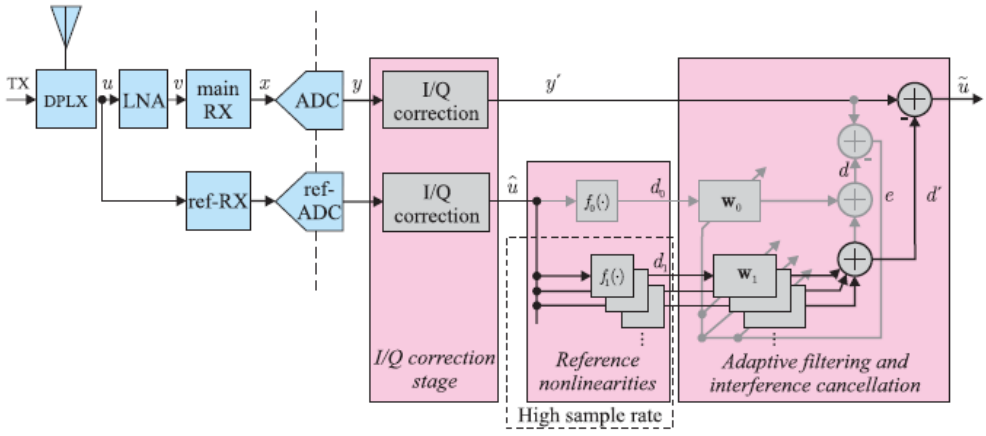

Figure 3.7: Principle of the RR-AIC technique. Reprinted from [32]

The reference-receiver-aided nonlinearity inversion (RR-INV) is implemented much the same way as the RR-AIC and it is shown in Figure 3.8. In the RR-INV approach, the linear reference signal is used as calibration signal. The goal here is to let the main path signal mimic the more linear behavior of the reference signal. The nonlinear models and the adaptive filters are used to find the reference nonlinearities that are capable of inverting the nonlinearities in the main path signal. Again, a major disadvantage of this

technique is that the accuracy of the hardware-specific nonlinear models used in modeling the nonlinear behavior of the front-end components immensely affects the calibration performance. Also, nonlinearities present in the reference signal will inadvertently end up appearing the calibrated signal. The number of required adaptive filters increase as the nonlinear components increase.

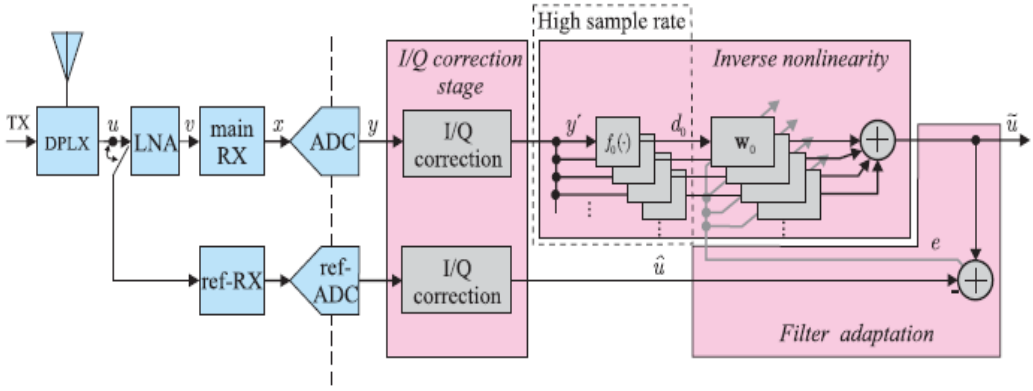

Figure 3.8: Principle of the RR-INV. Reprinted from [32]

In [60]–[62], a method that uses band-split filtering is introduced for multicarrier direct conversion receiver. It is shown in Figure 3.9. In this method, the received multicarrier signal is band-split into “channel of interest” and “other signals” or “other channels”. The lower branch in Figure 3.9 which contains the “other signals” is subjected to models of the nonlinearities prevailing in the upper branch signal. The idea is to regenerate the distorting intermodulation and harmonic components by means of nonlinear models. The output of the nonlinear models is filtered using an adaptive filter to scale the amplitude and phase of the generated nonlinear components and finally

subtracted from the upper branch signal to remove any nonlinearity. One disadvantage of this method is that it is channel specific and cannot band-select a wider range of frequency channels if the band-splitting filter is implemented in the analog domain since tunable yet highly selective analog filter design is difficult. Implementing the band-split filter in the digital domain would also put a stringent dynamic range and speed requirement on the ADC

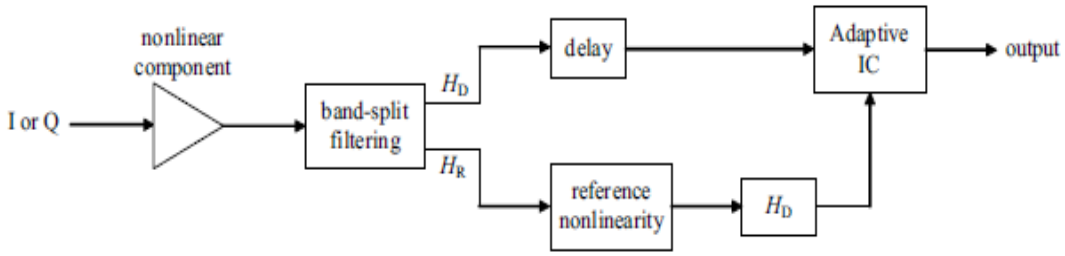

Figure 3.9: Band-split filtering method. Reprinted from [61]

In [63] and [64], a dual-path approach in which one path is used to catch the desired signal band and the other path is used to capture the blocker signal is proposed. It is illustrated diagrammatically in Figure 3.10. The LOs in both paths are tuned to different frequencies to appropriately down-convert the right signals to baseband, and the signals are then digitized using separate ADCs. The two signals are used together to remove nonlinear effects in two stages. In the first stage, an estimate of the nonlinearity parameters and the channel response are made. These estimates are then used in the second stage to recover the received data. A disadvantage of this method is that it

requires that the pilot sequence used in making channel estimates be correctly sampled. A consequence of this is that in adverse conditions a longer-than-normal sequence would be required for normal operation.

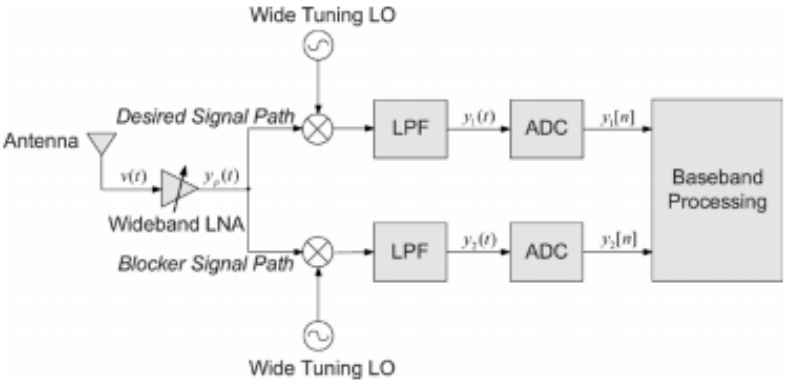

Figure 3.10: Digital Compensation technique. Reprinted from [63]

4 PROPOSED AUXILIARY-PATH-ASSISTED LINEARIZATION SOLUTION

This section provides details of the proposed auxiliary-path-assisted digital linearization technique. An auxiliary receiver path is employed in order to generate reference IM3 products in the digital domain for canceling third order nonlinear distortion. A very distinctive feature of this technique is that it is very simple to implement, and it works effectively in removing nonlinear distortions. The nonlinear suppression performance is verified via computer simulations and compared with state-of-the-art digital linearization techniques reported in literature.

4.1 Concept of the Proposed Solution

The system level structure of the proposed calibration technique is shown conceptually in Figure 4.1. It employs an auxiliary receiver path with a highly nonlinear low noise amplifier. The auxiliary path signal is essentially used in the digital domain for regenerating the nonlinear distortion components corrupting the main path signal. For this reason, a very nonlinear LNA, and hence a cheap off-the-self LNA, is used in the auxiliary path. This is a major advantage of the proposed scheme.

The proposed auxiliary-path-assisted linearization technique is a signal-amplitude-based technique, and has no inherent phase mismatch correction capability as in the case of adaptive interference cancellation used in previously described digital linearization

schemes. As a result, a separate phase mismatch correction scheme is added to cater for any delay between the main and the auxiliary path signals. This provides optimum calibration with the proposed technique. Two phase correction schemes are proposed; their known advantages and disadvantages are also well examined.

In the proposed linearization scheme, the digitized signals from the two paths are first phase corrected to remove time delays between the two paths. The phase-corrected data is then passed on to the core of the calibration scheme. As was stated earlier, the auxiliary path is used mainly in generating the distortion producing components. These nonlinear distortion components, specifically the third order distortion component, are generated with the right magnitude from the phase-corrected signals by means of two linearization coefficients K_1 and K_2, and other mathematical operations. In this way simple subtraction can be used to cancel out the nonlinear distortions in the main path signal. The linearization coefficients K_1 and K_2 are obtained by means of background adaptive filtering. Although the technique is developed to cancel out third order nonlinear distortion, it can be extended to cancel out higher order distortion components as well as even order distortion components.

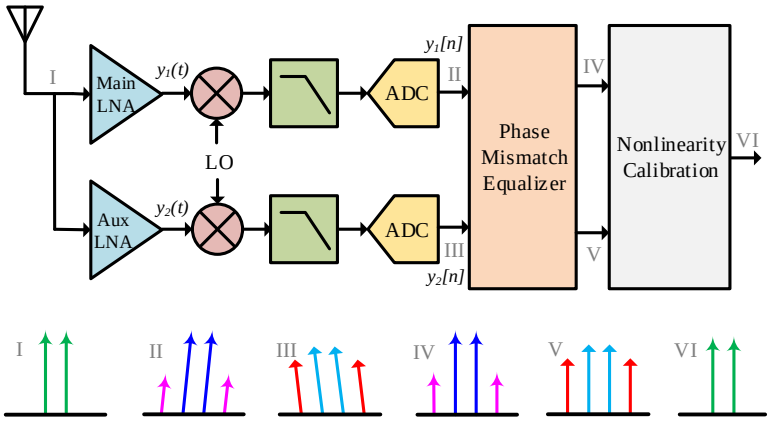

Figure 4.1: Block diagram of the proposed calibration technique

For simplicity and ease of understanding, the main and auxiliary LNAs are assumed to be modelled by the simplified equation in (*8*) repeated here for convenience.

$$y_1(t) = a_1 x(t) + a_3 x^3(t)$$
$$y_2(t) = b_1 x(t) + b_3 x^3(t) \quad (14)$$

where $y_1(t)$ and $y_2(t)$ are the outputs of the main and auxiliary paths, respectively. For such an LNA, the output for a two-tone signal will be given by (*15*). The third and fourth lines in (*15*) are the IM3 products. The fourth line IM3 products are the troublesome in-band IM3 products, and they are shown together with the fundamental two tones in the spectral example in Figure 4.1. The spectral example in Figure 4.1 demonstrates the effectiveness of the proposed scheme in cancelling out the fourth line IM3 products from the output signal. Later, simulation results will be used to show the effectiveness of the proposed linearization scheme in cancelling nonlinear distortions. The slanted spectral

lines in the spectral example II and III in Figure 4.1 simply demonstrate phase distortion difference between the main and auxiliary paths.

$$\begin{aligned} y(t) = &\left(a_1 + \frac{9a_3}{4}\right) cos(\omega_1 t) + \left(a_1 + \frac{9a_3}{4}\right) cos(\omega_2 t) \\ &+ \frac{a_3}{4} cos(3\omega_1 t) + \frac{a_3}{4} cos(3\omega_2 t) \\ &+ \frac{3a_3}{4} cos(2\omega_1 + \omega_2)t + \frac{3a_3}{4} cos(2\omega_2 + \omega_1)t \\ &+ \frac{3a_3}{4} cos(2\omega_1 - \omega_2)t + \frac{3a_3}{4} cos(2\omega_2 - \omega_1)t \end{aligned} \tag{15}$$

4.2 Algorithm Development

In this section, the methodology and ideology of the proposed linearization technique is discussed. We take a look at how the calibration is done using digital blocks in Figure 4.1 i.e. the phase mismatch equalizer and the nonlinearity calibration blocks.

4.2.1 Calibration algorithm

Figure 4.2 shows the dual-path receiver chain with the core of the proposed linearization technique. The main and auxiliary LNAs have different characteristics; the auxiliary LNA is more nonlinear in comparison with the main path LNA. This is one advantage of the proposed scheme. The main purpose of the auxiliary path is to

regenerate the third order nonlinear distortion components corrupting the main path signal.

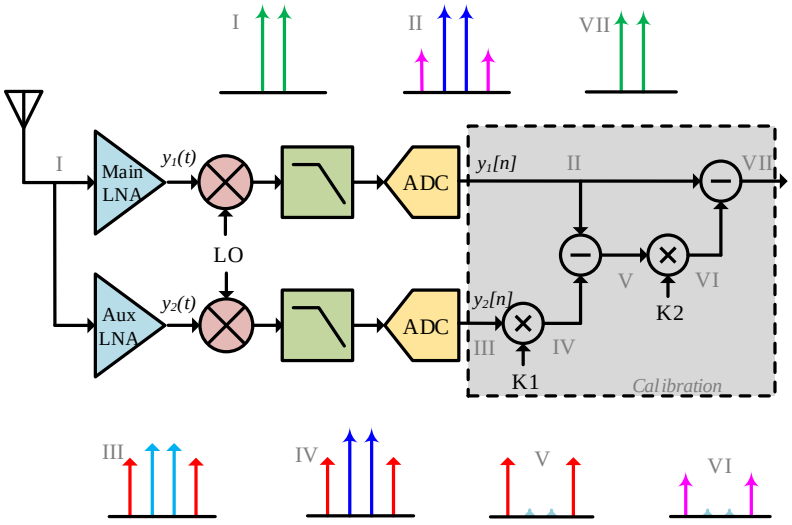

Figure 4.2: Core of the proposed calibration scheme

With the assumption that the RF signal structure is maintained in baseband, we have (*16*) from (*14*).

$$y_1[n] = a_1 x[n] + a_3 x^3[n]$$
$$y_2[n] = b_1 x[n] + b_3 x^3[n] \quad (16)$$

In order to generate the IM3 product – required for linearization – from the auxiliary path signal, the linear component (fundamental components) in the auxiliary path is eliminated. This is done by first multiplying the auxiliary path signal by the linearization coefficient K_1 such that its linear gain is the same as the linear components in the main path. K_1, then, is given by:

$$K_1 = \frac{a_1}{b_1} \tag{17}$$

For the parallel Hammerstein in (*4*), K_1 is given by (*18*). This expression is also valid in the case where the parameters are complex in nature.

$$K_1 = \frac{a_{1,0} + a_{1,1} + a_{1,2} + \cdots}{b_{1,0} + b_{1,1} + b_{1,2} + \cdots} = \frac{\sum_{q=0}^{Q} a_{1,q}}{\sum_{q=0}^{Q} b_{1,q}} \tag{18}$$

The auxiliary path signal after the multiplication becomes

$$K_1 y_2 = a_1 x[n] + K_1 b_3 x^3[n] \tag{19}$$

This new signal in (*18*) is then subtracted from the main path signal, theoretically leaving behind only IM3 products.

$$y_T = y_1 - K_1 y_2 = (a_3 - K_1 b_3) x^3[n] \tag{20}$$

The resulting IM3 product does not have the proper amplitude for canceling the IM3 products in the main path. Hence it is multiplied by another linearization coefficient, K_2. The linearization coefficient, K_2, boosts the amplitude of the resulting IM3 product such that its amplitude is the same as that of the main path's third order distortion term. K_2 is given by the following expression:

$$K_2 = \frac{a_3}{a_3 - K_1 b_3} \tag{21}$$

For the parallel Hammerstein in (*4*), K_2 is given by (*22*),.

$$K_2 = \frac{a_{3,0} + a_{3,1} + a_{3,2} + \cdots}{\left(a_{3,0} + a_{3,1} + a_{3,2} + \cdots\right) - K_1\left(a_{3,0} + a_{3,1} + a_{3,2} + \cdots\right)}$$

$$K_2 = \frac{\sum_{q=0}^{Q} a_{3,q}}{\sum_{q=0}^{Q} a_{3,q} - K_1\left(\sum_{q=0}^{Q} b_{3,q}\right)} \tag{22}$$

After the multiplication by K_2, the resultant IM3 signal, y_T, now becomes:

$$K_2 y_T = a_3 x^3[n] \tag{23}$$

This IM3 product generated from the auxiliary path signal is of the right amplitude to cancel out the third order distortion in the main path signal. This is demonstrated in Figure 4.2. The cancellation is done by means of simple subtraction between the main path signal and the resulting IM3 product, $K_2 y_T$, leaving behind a linearly amplified signal.

$$Output = y_1 - K_2 y_T = a_1 x[n] \tag{24}$$

The question that begs for an answer is, how are K_1 and K_2 determined? We answer this question in the next subsection.

4.2.2 K_1 and K_2 algorithm

The linearization coefficients, K_1 and K_2 are determined by means of adaptive filters. Adaptive filters in recent years have increasingly become an important tool in the fields

of communications, control, seismology, etc. Their uses include but not limited to, system identification, noise and echo cancellation, channel equalization and inverse system modeling. These filters are often referred to as the "self-designing" filters. They have a set of adjustable parameters with values that change automatically based on estimated statistics of the signals they process. The parameters change with the aim of minimizing an error function. The error function is the difference between a desired/reference signal and the filter output. The desired signal acts as a guide or frame of reference for adjusting the parameters in the adaptation process. The basic adaptive filter structure is shown in Figure 4.3, where *x(n)* is filter input, *y(n)* is the filter output, *d(n)* is the desired/reference signal, and *e(n)* is the error to be minimized. This basic structure is modified to suit the particular adaptive filtering application.

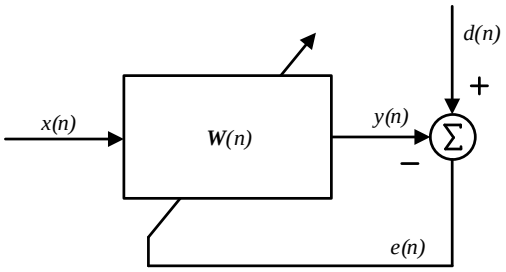

Figure 4.3: The basic adaptive filter

Adaptive algorithms are responsible for adjusting the filter parameters. These algorithms do not require a prior knowledge of the input signal, and hence their convergence to an optimum filter requires a sufficiently large number of iterations [65]. There are several optimization techniques for adjusting the filter parameters, examples

being, the recursive least-squares (RLS), the least mean-square (LMS) and its variants, etc.

In simple terms, the LMS algorithm uses the coefficient estimates at time *n* to estimate the coefficients at time *n+1* while the RLS algorithm uses the estimates at time *n-1* to estimate the coefficients at time *n*. the RLS algorithm has a high convergence speed. However, this high convergence speed is at cost of high computational complexity. The proposed technique has been implemented with both algorithms as well as the normalized LMS, and they all achieve high convergence accuracy. The LMS algorithm is described here and used in developing the basic algorithm for determining K_1 and K_2. The LMS algorithm is described by the equations given in (25) and (26), where μ is the step size. Full derivation of the algorithms can be found in [65]–[67].

$$e(n) = d(n) - y(n) = d(n) - \boldsymbol{w}^T(n)\boldsymbol{x}(n) \tag{25}$$

$$\boldsymbol{w}(n+1) = \boldsymbol{w}(n) + 2\mu e(n)\boldsymbol{x}(n) \tag{26}$$

The linearization coefficients, K_1 and K_2, are determined at the start-up of the receiver. They are determined individually as single adaptive filter coefficients by using two separate LMS algorithms. That is, the adaptive filters used in determining K_1 and K_2 have single coefficients that are adjusted using the LMS algorithm, and these filter coefficients are K_1 and K_2, the linearization coefficients. The LMS algorithms are employed one time, at the start-up of the receiver, in determining these coefficients.

With the coefficients stored, the LMS algorithms can be shut off, thereby saving power consumption.

The scheme for determining K_1 is shown in Figure 4.4. In this case the main path signal is used as the reference signal. The error function is used to adjust the single filter coefficient, which is K_1, to obtain an optimum filter solution. A quite linear signal is needed in determining K_1. Hence, a small amplitude signal is used. The processes involved in determining K_1 are described below.

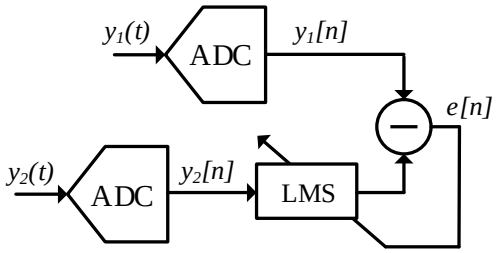

Figure 4.4: Adaptive algorithm for determining K_1

At the start of the receiver, a small amplitude single-tone signal at frequency f_1 is applied to the receiver. The output of the LNAs using (*14*) will be given by:

$$y_1(t) = \left(a_1 A + \frac{3}{4} a_3 A^3\right) \cos(w_1 t) + \frac{1}{4} a_3 A^3 \cos(3 w_1 t)$$
$$y_2(t) = \left(b_1 A + \frac{3}{4} b_3 A^3\right) \cos(w_1 t) + \frac{1}{4} b_3 A^3 \cos(3 w_1 t) \quad (27)$$

But since the amplitude, A, is very small, the outputs can be approximated to the linear signal in (*28*).

$$y_1(t) \approx a_1 A\cos(w_1 t)$$
$$y_2(t) \approx b_1 A\cos(w_1 t) \quad (28)$$

The LO frequency is then changed to f_1, and the signal is down-converted and digitized. In the digital domain, an LMS adaptive algorithm is used to calculate K_1 as the optimum filter coefficient from the digitized signal as shown in Figure 4.4. The determined K_1 is stored. In the LMS algorithm, K_1 is updated as:

$$K_1(n+1) = K_1(n) + 2\mu e(n)\boldsymbol{y_2}(n) \quad (29)$$

The final value of K_1 is stored. The LMS error to be minimized is given by:

$$e[n] = A(a_1 - K_1[n]b_1)\cos(w_1 nT) \quad (30)$$

K_2 is also calculated in a similar way. In this case a much less linear signal is needed at the output of the LNA, and hence a large amplitude signal is used. Specifically, we are interested in the products resulting from the cubic term in (*14*). The methodology for determining K_2 is shown in Figure 4.5.

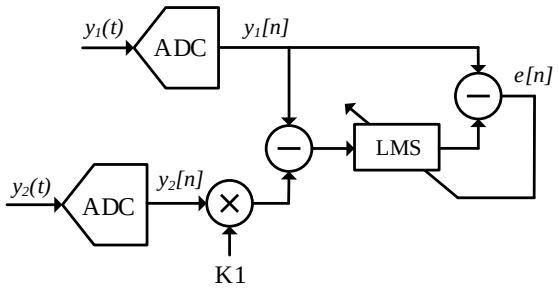

Figure 4.5: Adaptive algorithm for determining K_2

As the next step after determining and storing K_1, a large amplitude single-tone signal at frequency f_2 is passed through the receiver. In this case, the products of the cubic gain in (*14*) $\left(i.e.\frac{3}{4}a_3A^3 \; and \; \frac{1}{4}a_3A^3\right)$ become significant. In the digital domain, the auxiliary path signal is multiplied by the already-determined K_1, and then subtracted from the main path signal so as to eliminate the fundamental component resulting from the linear gain. Again, using an LMS adaptive filter, K_2 is determined as the optimum filter solution. K_2 is also stored. K_2 is updated as follows:

$$K_2(n+1) = K_2(n) + 2\mu e(n)(\boldsymbol{y_1}[n] - K_1\boldsymbol{y_2}[n]) \tag{31}$$

The LMS error to be minimized is given by:

$$e[n] = A^3 * \{a_3 - (a_3 - K_1b_3)K_2[n]\} * \cos^3(w_1n) \tag{32}$$

The closer the error functions in (*31*) and ((*32*) are to zero, the closer K_1 and K_2 in (*29*) and (*31*) would be to their ideal values in (*17*) and (*21*), respectively. Same situation applies to case of the parallel Hammerstein models.

Figure 4.6 and Figure 4.7 show the RLS convergence speed for the LNA and general receiver specifications used in [32]. More light will be thrown on this receiver characteristics and the corresponding auxiliary path characteristics in the results section. K_1 converges with high accuracy after roughly 700 iterations. With the already determined K_1, K_2 is also determined. It is seen to have high convergence speed and accuracy.

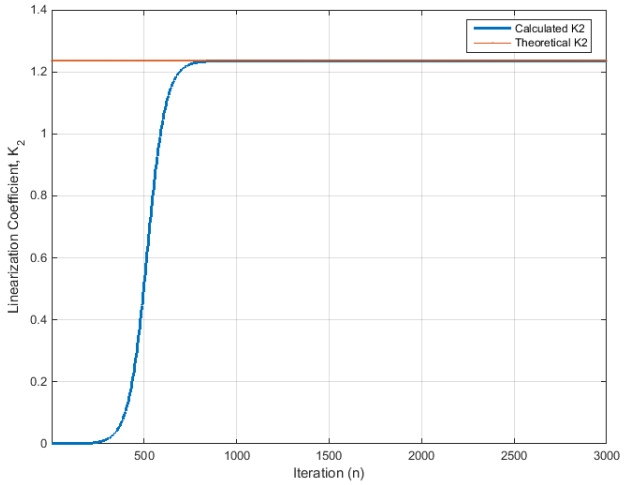

Figure 4.6: RLS convergence rate for K_1

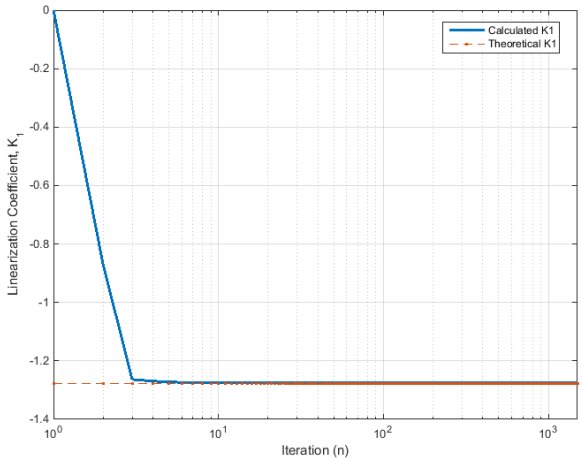

Figure 4.7: RLS convergence rate for K_2

Figure 4.8 and Figure 4.9 show the determined K_1 and K_2 accuracy as a function of the initial signal amplitude used in calculating these coefficients for the LNA in [32]. The accuracy of K_1 deteriorates as the initial signal amplitude increases. In the case of K_2, accuracy is poor for lower signal amplitudes; it gets better for input signal powers above -5 dBm. With such plots for a particular LNA, the right signal amplitudes can be determined to give high accuracy in determining K_1 and K_2.

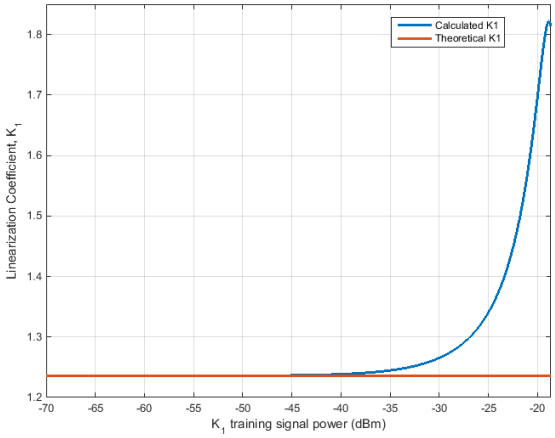

Figure 4.8: K_1 accuracy as a function of training signal amplitude

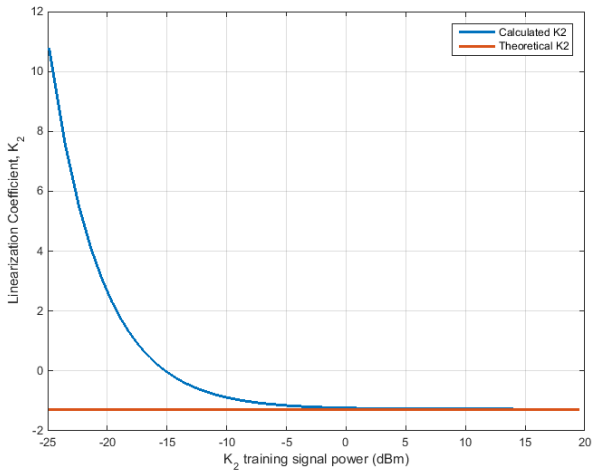

Figure 4.9: K_1 accuracy as a function of training signal amplitude

4.2.3 Phase correction algorithm

From the discussions about the proposed linearization technique, it can be seen that the proposed technique is a purely signal-amplitude-based technique. As such, its performance suffers in the event of phase mismatch (or time delay) between the two paths. Figure 4.10 shows the proposed technique's sensitivity to phase mismatch between the two receiver paths. The proposed technique can achieve up to 30 dBm in IIP3 performance but this performance degrades with increasing phase delays between the two paths. The phase/time delays are due to the fact that no two circuit components are the same, a major consequence of the ever-present PVT variations. Moreover, it is per design that the auxiliary path LNA be different from the main path LNA; the

proposed technique banks on a more nonlinear auxiliary path, and hence phase mismatch is an unavoidable consequence.

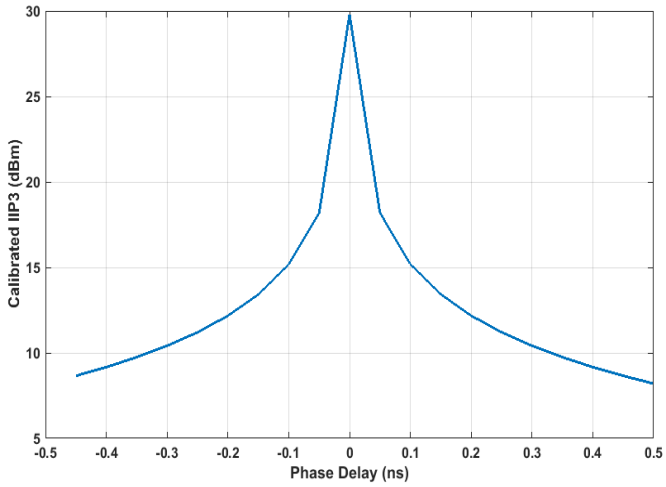

Figure 4.10: Linearization scheme sensitivity to phase mismatch

Assuming that the phase mismatch between the two paths only occurs on the auxiliary path, the LNAs in (*14*) will have the following outputs for a single tone signal:

$$\begin{aligned} y_1(t) &= a_1 sin(\omega_0 t) + a_3 sin^3(\omega_0 t) \\ y_2(t) &= b_1 sin(\omega_0 t + \varphi) + b_3 sin^3(\omega_0 t + \varphi) \end{aligned} \tag{33}$$

where φ is the phase difference between the two paths. If the phase mismatch, φ, is small, then the output of the auxiliary path can be written as:

$$\begin{aligned} y_2(t) = b_1[sin(\omega_0 t) + \varphi \cos(\omega_0 t)] \\ + b_3[sin^3(\omega_0 t) + 3\sin^2(\omega_0 t) co\, s(\omega_0 t)] \end{aligned} \tag{34}$$

Now, if the proposed calibration technique described in (*17*)-(*24*) is used to cancel out the harmonic components without any form of phase correction, the following uncancelled error will result at the end of the calibration process:

$$error = \varphi a_1 K_2 cos(\omega_0 t) + \varphi \frac{3a_1 b_3}{b_1} K_2 \sin^2(\omega_0 t) co\, s(\omega_0 t) \qquad (35)$$

These uncancelled terms cause performance degradation in the calibration scheme as show in Figure 4.10. The performance degradation worsens for higher phase mismatches and higher K_2 values.

In this work, two simple phase correction techniques are proposed along with the calibration scheme for optimum linearization performance. These are the fast Fourier transform (FFT) based phase compensation and the zero-phase filtering phase compensation. The FFT based phase delay compensation is shown in Figure 4.11. In this phase calibration scheme, the phase mismatch correction is done by first taking the FFT of the main and auxiliary path signals. For a periodic signal *x(t)* with period $T_0 = 1/f_0$, the Fourier series expansion is given by (*36*), where *n = 0, 1, 2, 3, …*

$$x(t) = \sum_{n=-\infty}^{\infty} c_n e^{j2\pi n f_0 t} \qquad (36)$$

The coefficients, c_n, are related to *x(t)* by

$$c_n = \frac{1}{T_0}\int_{t}^{t+T_0} x(t)e^{-j2\pi n f_0 t}dt \tag{37}$$

The coefficients, which are complex in general, can be expressed as

$$c_n = |c_n|e^{j\arg(c_n)} \tag{38}$$

where *arg(c_n)* is the angle of c_n. It defines the phase spectrum. The phase extractor (PE) in the FFT-based phase correction scheme is used to estimate the sample-by-sample phase difference between the two paths from the phase spectrum. With the main path signal considered as a reference and the auxiliary path signal as the signal whose phase is to be corrected, the estimated phase difference is used to adjust the phase of the auxiliary path signal in the phase controller (PC). This is also done sample-by-sample wise using the estimated sample-by-sample phase difference. At this point, the phase of the auxiliary path signal should be almost the same as that of the main path signal. Inverse Fourier transform is then taken and the signal is passed on to the calibration scheme. This phase correction scheme matches the phases of the two paths. It does not consider phase mismatch with respect to the originally received signal.

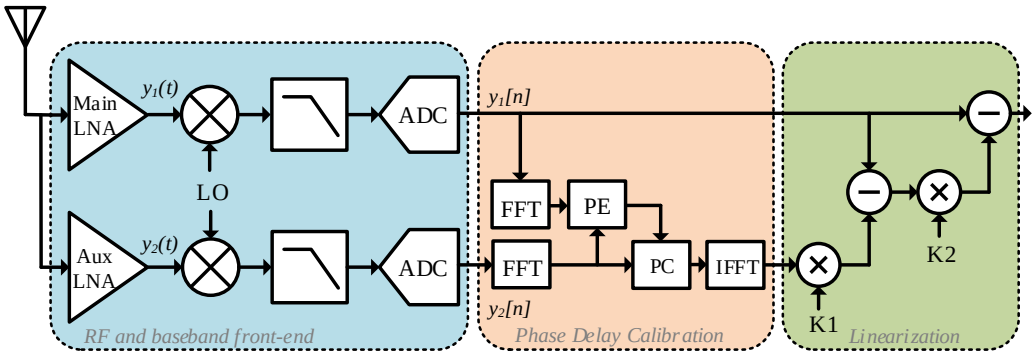

Figure 4.11: FFT based phase delay compensation

Now, we take a look at the zero-phase filtering approach. The nonlinear phase effects can be cancelled by following the process shown in Figure 4.12. It performs zero-phase filtering by using the same filter twice. In the following discussion, the filters are assumed to add a phase shift of φ, and the time reversal processes induce a phase shift of β. For an input data with an arbitrary phase of θ, the first filter will add a phase shift φ, and the total phase at point K will be $\theta - \varphi$. The first time-reversal will induce a phase of β, and the total phase at point L will be $\theta - \varphi - \beta$. The second filter will also induce a phase shift of φ but since it filters the time reversed data, it nullifies the phase of the first filter. Hence the total phase shift at point M is $\theta - \beta$. The second time-reversal process also nullifies the phase shift of the first time-reversal process and the phase of the output signal will be θ, just as was with the original signal.

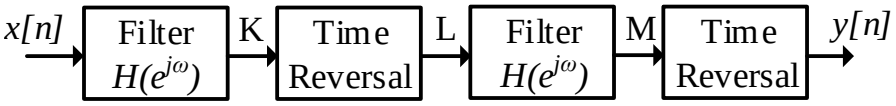

Figure 4.12: Zero phase filtering technique

Mathematically, the operation of the zero-phase filtering is expressed below. When an input signal *x[n]* is passed through a filter with real coefficient $H(e^{j\omega})$, the output signal, $K(e^{j\omega})$, is given by:

$$K(e^{j\omega}) = X(e^{j\omega})H(e^{j\omega}) \tag{39}$$

If this data is saved and time reversed, the new reversed output will be the conjugate of the original data. Hence, we will have:

$$L^*(e^{j\omega}) = X^*(e^{j\omega})H^*(e^{j\omega}) = X(e^{-j\omega})H(e^{-j\omega}) \tag{40}$$

Now, if this output is subjected to the same filter $H(e^{j\omega})$ again, the new output, denoted as *M(n)*, will be given by;

$$M(n) = X(e^{-j\omega})H(e^{-j\omega})H(e^{j\omega}) = X(e^{-j\omega})\left|H(e^{j\omega})\right|^2 \tag{41}$$

Time reversing the new data, *M(n)* would remove the phase shift introduced by the first time-reversal. The final output would be given by:

$$Y(e^{j\omega}) = X(e^{j\omega})\left|H(e^{j\omega})\right|^2 \tag{42}$$

This output is purely real-valued and therefore has zero phase or phase distortions.

Figure 4.13 shows the zero-phase filtering technique being used as a phase mismatch correction technique in the proposed linearization scheme. This phase mismatch correction technique involves correcting the phase of the individual paths with respect to the received data. That is, phase distortions introduced by the main and auxiliary receiver paths are cancelled out individually, and the resulting signals would have the same phase as the received signal. This results in zero phase delay between the main and the auxiliary path signals.

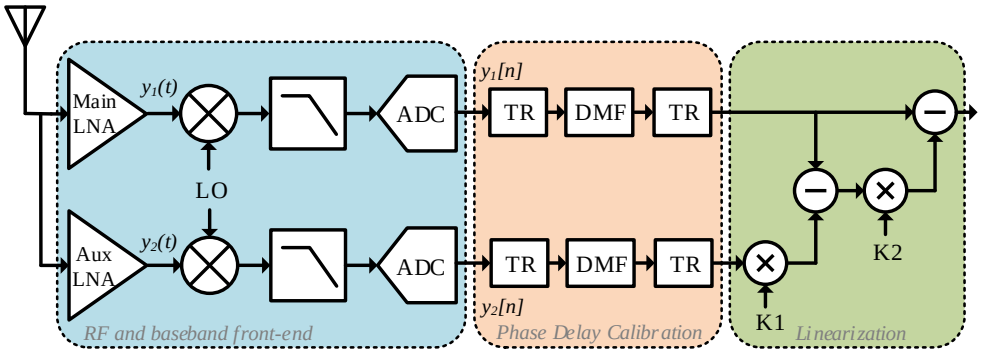

Figure 4.13: Zero-phase filtering based phase delay calibration

With this phase correction technique, the individual RF and baseband front-ends of the two receiver paths (main and auxiliary receiver paths) form the first filter of the zero-phase filter in Figure 4.12. That is, each receiver front-end is considered as a separate filter. The "filter" transfer functions of these front-ends are replicated in the digital domain to form the second filter of the zero-phase filter in Figure 4.12. Thus, any received data is first "filtered" by the receiver front ends, time reversed in the digital domain and passed through a digitally matched filter (DMF), which is a digital replica of

the front-end frequency characteristics. The output of the DMF is time reversed again, thus, completing the cycle of zero-phase filtering in Figure 4.12. The resulting signals in the main and auxiliary paths have the same phase as the received signal, signifying the removal of phase distortions introduced by the individual paths.

The DMF filter coefficients are also determined at the start of the receiver. To do this, a known ideal waveform is stored in the digital domain. An analog version of this waveform is passed through the receiver and collected at the output of the ADC. An adaptive algorithm is used to fit the received data unto the known data, and the optimum adaptive filter solution is the equivalent DMF. An adequate number of filter coefficients should be chosen to fully represent all the analog domain effects especially phase mismatches.

4.2.4 Practical aspects of phase correction

The previous subsection described techniques for mitigating phase mismatches between the main and the auxiliary paths. We now consider some practical limitations of these techniques.

Regarding the FFT based, it is important to make sure that the number of samples is high enough during the FFT processing. This is necessary in order to clearly distinguish between any two individual tones that are close together. The number of samples may be

temporarily increased by interpolation. It should be noted that this is only required in the FFT processing and does not affect the actual ADC sampling rate. It should also be noted that FFT processing can be computationally intensive. This fact should be taken into consideration as a cost in implementing the FFT-based phase correction.

Concerning the zero-phase filtering technique, it is important to understand its practicalities as far as real-time systems are concerned. Since zero-phase filtering involves time reversal of the data, it is not practical in real-time systems as it would mean the system has be non-causal (that is, capable of predicting future samples). In this case, the proposed zero-phase technique becomes much useful in offline signal systems. However, this limitation makes it very suitable for some digital modulation schemes such as OFDM, where data is processed in chunks/blocks. Simulation results on an OFDM system will be used to demonstrate this point.

Yet another practical aspect to be consider concerning the phase mismatch correction using the zero-phase filtering technique is in determining the number of DMF coefficients to fully capture the behavior of the receiver front-end components. As a rule of thumps, the largest possible number of coefficients should always be used. It is worth noting that the training of the DMF coefficients using adaptive algorithm needs to be done once. Once the coefficients are determined, they can always be used without further tuning with the adaptive filter.

4.3 Results

In this subsection, simulation results showing the performance of the proposed linearization technique are presented. First, specific tests are performed on the proposed technique to ascertain its performance, and then other tests are performed to compare the proposed technique to other state-of-the-art techniques. The receiver parameters used for these tests are listed in Table 1. Changes to these parameters will be stated accordingly.

Table 1: Receiver Parameters

Parameter	Value
Baseband bandwidth	100 MHz
ADC resolution	12 bits
$G_{LNA,main}$	30 dB
$IIP3_{LNA,main}$	1 dBm
$G_{LNA,aux}$	26 dB
$IIP3_{LNA,aux}$	-12 dBm
Phase mismatch	4^0
Memory depth	Third order memory depth using three-tap adaptive filters per LNA coefficient

In order to test and quantify the IIP3 performance of the proposed linearization technique, a two-tone test was performed. A two-tone signal with frequencies components at 17 MHz and 20 MHz is passed through the main and auxiliary receiver chains. Figure 4.14 (a) shows the two-tone signal with the troublesome in-band third order intermodulation terms at 14 MHz and 23 MHz. The other spectral components are the high frequency third harmonics (51 MHz and 60 MHz), and the high frequency third order intermodulation products (54 MHz and 57 MHz). Figure 4.13(b) shows the

linearized or calibrated signal. As seen from the figure, the proposed technique removes all products of the cubic term in (*14*) including the third harmonic, a useful feature to have in the area of intra-band carrier aggregation. The proposed linearization technique can achieve up to 30 dBm in IIP3.

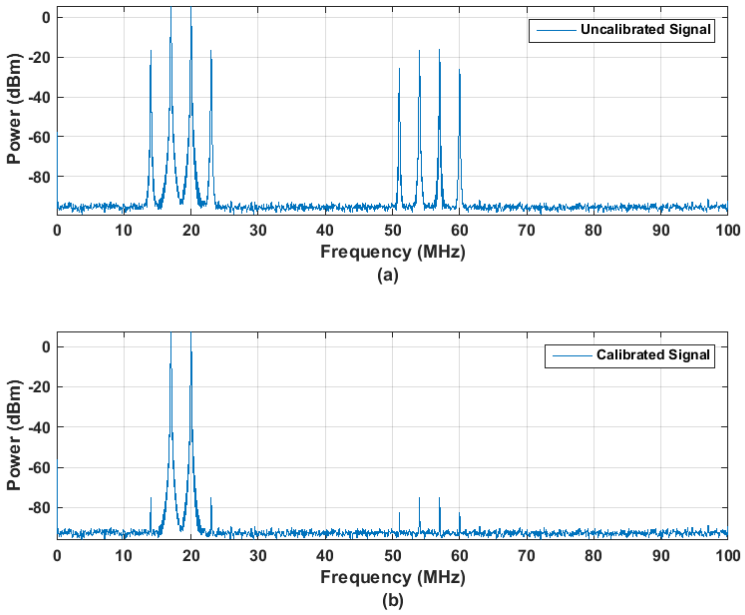

Figure 4.14: (a) Uncalibrated two-tone spectrum (b) Calibrated two-tone spectrum

Next, the necessity of having a nonlinear auxiliary path is examined. In this test scenario, both LNAs are assumed to have the same linear gains of 30 dB, and the IIP3 of the auxiliary path is varied. The results are shown in Figure 4.15. It can be seen from the results that as the auxiliary LNA becomes more nonlinear, the IIP3 performance increases. This behavior is expected because one of the main purposes of the auxiliary LNA is to reproduce the nonlinear term corrupting the main path. It is also expected that

the linearization performance degrades as the characteristics of the two LNAs become the same. This is an indication that a less expensive nonlinear LNA can be used in the auxiliary path for optimum results. From the results shown in Figure 4.15, it can also be seen that another bottle to the linearization performance is the resolution of the ADC used; the higher the resolution, the higher the measured IIP3.

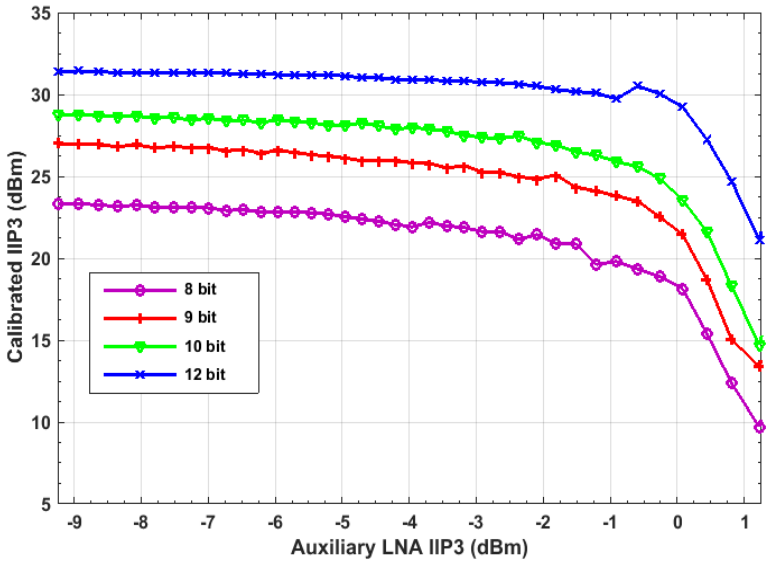

Figure 4.15: Measured IIP3 vs auxiliary path LNA nonlinearity, and ADC resolution

Experiments were also done to test the performance of the zero-filtering based phase calibration system using orthogonal frequency division multiplexing (OFDM) systems. OFDM systems allows high data rates in wireless systems, and provides high resilience to interference and multipath fading. However, a major pitfall of OFDM systems is that their multicarrier signals a high peak-to-average power ratios (PAPR) which may lead to severe nonlinear distortions.

In this experiment, we use OFDM signal with QPSK modulated subcarriers. 128 subcarriers were used. The symbol rate was 600 kHz. Similar QPSK modulated signal were used at the start-up of the receiver to obtain the DMF coefficients. MATLAB's LMS filter function was used to obtain a 24-coefficient DMF.

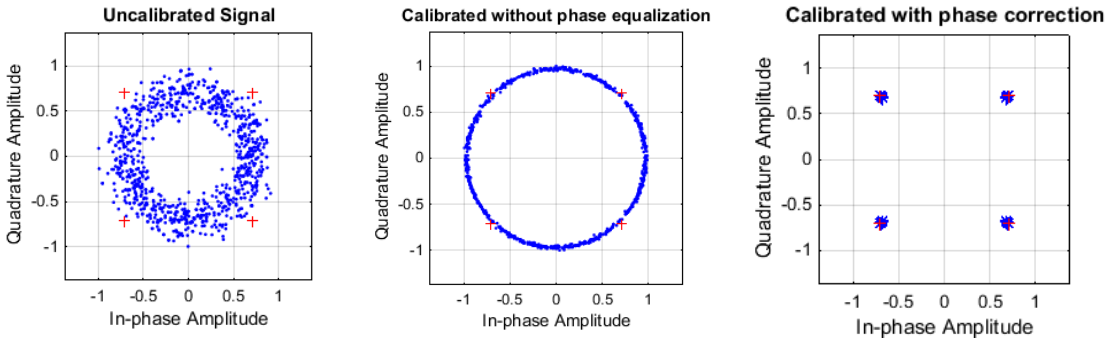

Figure 4.16: OFDM constellation diagram

Figure 4.16 shows the constellation diagram obtained from this experiment. The figure to the left is the received signal without any linearization technique applied. The measured RMS error vector magnitude (EVM_{rms}) is 29.33%. The figure in the middle shows the linearized OFDM signal without any phase correction. It gives an EVM_{rms} of 11.54%. The results on the right is obtained by first using the zero-phase filtering phase correction technique before calibration. The measured (EVM_{rms}) is 3.84% - a close to perfect QPSK constellation.

Tests in which the test scenarios and LNA parameters used in [10] and [32] are used were also performed to compare the proposed technique to the-state-of-art techniques. The test as well as the results are discussed here.

In [10] the modified two-tone IIP3 test is used to assess IM3 calibration. This test is a reflection of the reality that the UMTS blocking test is a two-tone test with a modulated TX leakage from the antenna duplexer being one of the tones. In this case, the other tone is a CW blocker. The main path LNA characteristics are chosen to conform to that used in [10] i.e. G_{LNA} = 17 dB and $IIP3_{LNA}$ = +16 dBm. Based on this, the gain and IIP3 of the auxiliary path LNA are chosen to be 14 dB and +4 dBm, respectively. The results for the modified two-tone test using the proposed linearization technique and that proposed in [10] are shown in Figure 4.17. The lumped input-referred error, which accounts for gain loss and residual IM products, is measured for different blocker powers. The plots include performance under worst-case blocker conditions for the duplexer used in [10]. As can be seen from the results, the proposed technique is up to par with the technique proposed in [10] even without phase mismatch correction. When phase mismatch correction is introduced in the proposed technique, we see a much greater suppression in the input-referred error.

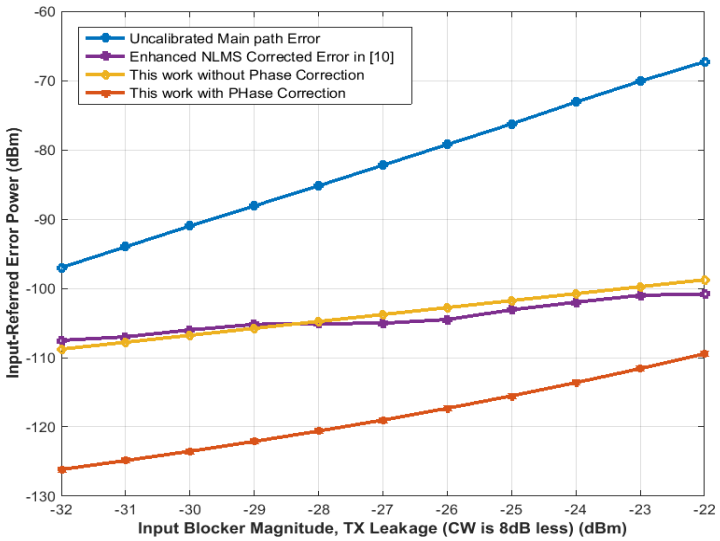

Figure 4.17: Measured modified two-tone performance of receiver

Next, we also perform the test use in [32]. In this test scenario, a weak LTE uplink carrier with a 10 MHz bandwidth is received together with two strong blocking carriers (each also having a 10 MHz bandwidth) such that the weak LTE signal suffers from nonlinear distortion produced by the strong blocker signals. As in [32], the weak LTE carrier, after down-conversion, is located at the IF center frequency of 20MHz, and the strong blocker carriers are located at 10 and 40MHz. In this way, the third order distortion component around -20 MHz, with its characteristic triple bandwidth, falls atop the weak carrier signal. Again, for fairness of comparison, the main path LNA gain and IIP3 are chosen to be 22 dB and -7 dBm, respectively, as in [32]. The reception bandwidth is 100MHz. The measured SNDRs for the weak LTE signal as a function of the blocker power with our linearization technique and the two techniques proposed in [32] are shown in Figure 4.18. It can be seen from this figure that the SNDR suffers with

increasing blocker power as is usually the case for profiles dominated by nonlinear distortion.

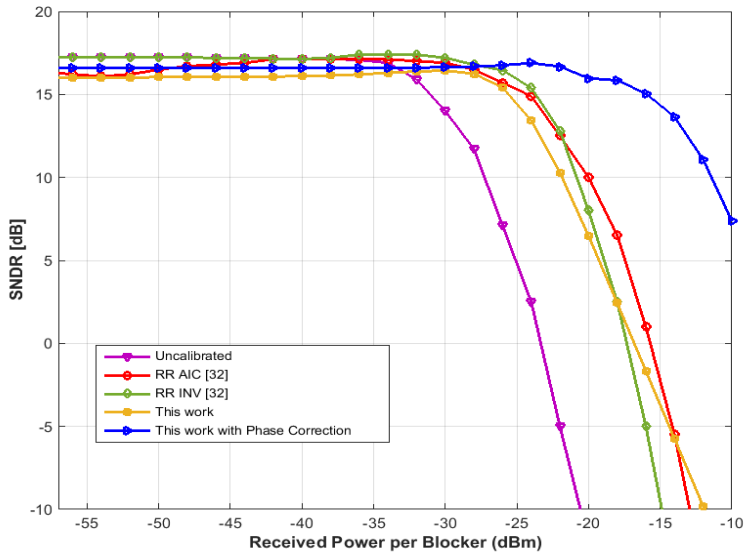

Figure 4.18: Measured SNDR as a function of RF blocker power

As was stated in [32], the RR-INV slightly outperforms the RR-AIC, and both techniques generally give 1-to-2 dB more SNDR at low blocker powers in comparison to the proposed technique. However, the proposed technique is more tolerant and robust to higher blocker power compared to the no-linearization case and both techniques in [32]. From the weak LTE signal point of view, the blocker tolerance compared with no linearization at all is improved by 7.0 dBm with RR-AIC and 7.5 dBm with RR-INV at 14 dB SNDR. However, the blocker tolerance is improved by 14.9 dBm with the proposed technique at 14 dB SNDR. Concurrently, at -15 dBm of blocker power which is a test scenario specified by 3GPP [68], the SNDR measured for no linearization is -

32.5 dB, and -2.5 dB and -9 dB for RR-AIC and RR-INV, respectively. However, the proposed technique achieves up to +14.3 dB SNDR at this high blocker power, roughly 3 dB less than its SNDR at lower blocker power. In general, all the said linearization techniques achieve similar SNDR at lower blocker powers but the proposed technique has a higher tolerance to increasing blocker power.

4.4 Comparison of Results

Table 2 compares the performance of the proposed linearization technique to some existing techniques in literature. The proposed calibration technique can achieve better IIP3 performance in comparison to other works in literature.

Table 2: Table of comparison

Parameter	**This work**	[10]	[32]	[46]	[39]
IIP3 (dBm)	Up to +30	+5.3	-	+10.5	+18
SNDR at -15 dBm blocker power (dBm)	+14.3	-	-9	-	-
ADC Resolution	12 bits	8 bits	12 bits	-	-
Bandwidth (MHz)	100	23	100	-	-

5 CONCLUSION

In this thesis work, an auxiliary-path-assisted digital linearization technique was presented. The presented linearization technique was specifically developed with the aim of cancelling out third order intermodulation products as well as third order harmonics. The presented technique can be extended to cancel out second order, as well as higher order intermodulation and harmonic terms. Two phase equalization techniques for handling the inadvertent phase mismatches between the two signal paths were also introduced. Computer-based simulation results were also presented. To ensure that the presented technique is capable of handling real-life intermodulation and harmonic distortions, in-depth LNA models which included memory effects were employed in all the tests.

The presented linearization technique can achieve IIP3 performance up to +30 dBm with a major performance bottleneck being the resolution of the ADC used. Another parameter that affects the performance of the presented linearization scheme is the linearity of the auxiliary LNA path used. It is preferred that the auxiliary path LNA be more nonlinear in comparison with the main path LNA.

The presented technique shows strong blocker tolerance with little performance degradation, compared with some state-of-the-art techniques. The presented linearization technique can be used in many applications; a particularly useful one being in the area of carrier aggregation and cognitive radios.

REFERENCES

[1] M. Kitsunezuka, K. Kunihiro, and M. Fukaishi, "Efficient Use of the Spectrum," *IEEE Microw. Mag.*, vol. 13, no. 1, pp. 55–63, Jan. 2012.

[2] Y.-C. Liang, K.-C. Chen, G. Y. Li, and P. Mahonen, "Cognitive radio networking and communications: an overview," *IEEE Trans. Veh. Technol.*, vol. 60, no. 7, pp. 3386–3407, Sep. 2011.

[3] M. Allen, "Nonlinear distortion in wideband radio receivers and analog-to-digital converters: modeling and digital suppression," 2015.

[4] B. Razavi, "Design considerations for direct-conversion receivers," *IEEE Trans. Circuits Syst. II Analog Digit. Signal Process.*, vol. 44, no. 6, pp. 428–435, Jun. 1997.

[5] M. Valkama, J. Pirskanen, and M. Renfors, "Signal processing challenges for applying software radio principles in future wireless terminals: an overview," *Int. J. Commun. Syst.*, vol. 15, no. 8, pp. 741–769, Oct. 2002.

[6] M. Valkama, *Advanced I/Q signal processing for wideband receivers: models and algorithms*. 2001.

[7] G. Fettweis, M. Löhning, D. Petrovic, M. Windisch, P. Zillmann, and W. Rave, "Dirty RF: A New Paradigm," *Int. J. Wirel. Inf. Networks*, vol. 14, no. 2, pp. 133–148, Jun. 2007.

[8] P. Rykaczewski, D. Pienkowski, R. Circa, and B. Steinke, "Signal path

optimization in software-defined radio systems," *IEEE Trans. Microw. Theory Tech.*, vol. 53, no. 3, pp. 1056–1064, Mar. 2005.

[9] P.-I. Mak, S.-P. U, and R. Martins, "Transceiver architecture selection: Review, state-of-the-art survey and case study," *IEEE Circuits Syst. Mag.*, vol. 7, no. 2, pp. 6–25, 2007.

[10] E. A. Keehr and A. Hajimiri, "Equalization of Third-Order Intermodulation Products in Wideband Direct Conversion Receivers," *IEEE J. Solid-State Circuits*, vol. 43, no. 12, pp. 2853–2867, Dec. 2008.

[11] H. Darabi, "A Blocker Filtering Technique for SAW-Less Wireless Receivers," *IEEE J. Solid-State Circuits*, vol. 42, no. 12, pp. 2766–2773, Dec. 2007.

[12] S. Pourbagheri, K. Mayaram, and T. S. Fiez, "A self-clocked blocker-filtering technique for SAW-less wireless applications," in *2016 IEEE Radio Frequency Integrated Circuits Symposium (RFIC)*, 2016, vol. 2016–July, pp. 250–253.

[13] N. K. Yanduru *et al.*, "A WCDMA, GSM/GPRS/EDGE Receiver Front End without Interstage SAW Filter," in *IEEE Radio Frequency Integrated Circuits (RFIC) Symposium, 2006*, 2006, pp. 9–12.

[14] B. Tenbroek *et al.*, "Single-Chip Tri-Band WCDMA/HSDPA Transceiver without External SAW Filters and with Integrated TX Power Control," in *2008 IEEE International Solid-State Circuits Conference - Digest of Technical Papers*, 2008, vol. 51, pp. 202–607.

[15] A. A. Abidi, "Direct-conversion radio transceivers for digital communications,"

IEEE J. Solid-State Circuits, vol. 30, no. 12, pp. 1399–1410, 1995.

[16] J. Crols and M. S. J. Steyaert, "Low-IF topologies for high-performance analog front ends of fully integrated receivers," *IEEE Trans. Circuits Syst. II Analog Digit. Signal Process.*, vol. 45, no. 3, pp. 269–282, Mar. 1998.

[17] J. Laskar, B. Matinpour, and S. Chakraborty, *Modern Receiver Front-Ends*. Hoboken, NJ, USA: John Wiley & Sons, Inc., 2004.

[18] M. J. Buckingham, *Noise in Electronic Devices and Systems*. New York: E. Horwood, 1983.

[19] K. Kawakami, K. Tajima, M. Shimozawa, K. Itoh, N. Kasai, and A. Iida, "Fully monolithic integrated even harmonic quadrature ring mixer with an active matched 90 degree power divider for direct conversion receivers," in *1997 IEEE MTT-S International Microwave Symposium Digest*, 1997, vol. 2, pp. 657–660.

[20] A. Rofougaran, J. Y.-C. Chang, M. Rofougaran, and A. A. Abidi, "A 1 GHz CMOS RF front-end IC for a direct-conversion wireless receiver," *IEEE J. Solid-State Circuits*, vol. 31, no. 7, pp. 880–889, Jul. 1996.

[21] K. Dufrene and R. Weigel, "Adaptive IP2 calibration scheme for direct-conversion receivers," *IEEE Radio Wirel. Symp.*, pp. 111–114, 2006.

[22] Hangjun Chen and A. M. Haimovich, "Iterative estimation and cancellation of clipping noise for OFDM signals," *IEEE Commun. Lett.*, vol. 7, no. 7, pp. 305–307, Jul. 2003.

[23] M. Faulkner, "DC offset and IM2 removal in direct conversion receivers," *IEE*

Proc. - Commun., vol. 149, no. 3, pp. 179–184, Jun. 2002.

[24] Hsing-Hung Chen, Po-Chiun Huang, Chao-Kai Wen, and Jiunn-Tsair Chen, "Adaptive compensation of even-order distortion in direct conversion receivers," in *2003 IEEE 58th Vehicular Technology Conference. VTC 2003-Fall (IEEE Cat. No.03CH37484)*, 2003, p. 271–274 Vol.1.

[25] "Universal Mobile Telecommunications System (UMTS); Base Station (BS) radio transmission and reception (FDD)," no. 3GPP TS 25.104 version 11.8.0 Release 11.

[26] Behzad Razavi, *RF Microelectronics*, 2nd ed. Upper Saddle River, NJ: Pearson, 2012.

[27] P. B. Kenington, *High-linearity RF amplifier design*. Norwood, MA: Artech House, 2000.

[28] J. C. Pedro and S. A. Maas, "A comparative overview of microwave and wireless power-amplifier behavioral modeling approaches," *IEEE Trans. Microw. Theory Tech.*, vol. 53, no. 4, pp. 1150–1163, Apr. 2005.

[29] S. C. Cripps, *RF Power Amplifiers for Wireless Communications*, vol. 40, no. 6. Artech House, 2006.

[30] P. Landin, *On Radio Frequency Behavioral Modeling*. 2009.

[31] "HD24089 500 – 6000MHz Low Noise Amplifier." [Online]. Available: http://www.rfcomp.com/download/product_specs/low_noise/HD24089specs.pdf.

[32] J. Marttila, M. Allen, M. Kosunen, K. Stadius, J. Ryynanen, and M. Valkama,

"Reference Receiver Enhanced Digital Linearization of Wideband Direct-Conversion Receivers," *IEEE Trans. Microw. Theory Tech.*, vol. 65, no. 2, pp. 607–620, Feb. 2017.

[33] S. Ali and E. Arabi, "Behavioral modeling of RF front end devices in Simulink," 2008.

[34] D. R. Morgan, Z. Ma, J. Kim, M. G. Zierdt, and J. Pastalan, "A Generalized Memory Polynomial Model for Digital Predistortion of RF Power Amplifiers," *IEEE Trans. Signal Process.*, vol. 54, no. 10, pp. 3852–3860, Oct. 2006.

[35] Hyunchul Ku and J. S. Kenney, "Behavioral modeling of nonlinear RF power amplifiers considering memory effects," *IEEE Trans. Microw. Theory Tech.*, vol. 51, no. 12, pp. 2495–2504, Dec. 2003.

[36] H. Zhang and E. Sanchez-Sinencio, "Linearization Techniques for CMOS Low Noise Amplifiers: A Tutorial," *IEEE Trans. Circuits Syst. I Regul. Pap.*, vol. 58, no. 1, pp. 22–36, Jan. 2011.

[37] V. Aparin and L. E. Larson, "Linearization of monolithic LNAs using low-frequency low-impedance input termination," *Eur. Solid-State Circuits Conf.*, vol. 1, pp. 137–140, 2003.

[38] V. Aparin and C. Persico, "Effect of out-of-band terminations on intermodulation distortion in\ncommon-emitter circuits," *1999 IEEE MTT-S Int. Microw. Symp. Dig. (Cat. No.99CH36282)*, vol. 3, pp. 2–5, 1999.

[39] Y. Ding and R. Harjani, "A +18 dBm IIP3 LNA in 0.35 μm CMOS," *IEEE Int.*

Solid-State Circuits Conf., p. 162–163, 2001.

[40] T. W. Kim, "A Common-Gate Amplifier With Transconductance Nonlinearity Cancellation and Its High-Frequency Analysis Using the Volterra Series," *IEEE Trans. Microw. Theory Tech.*, vol. 57, no. 6, pp. 1461–1469, Jun. 2009.

[41] B. Kim, J.-S. K. J.-S. Ko, and K. Lee, "Highly linear CMOS RF MMIC amplifier using multiple gated\ntransistors and its Volterra series analysis," *2001 IEEE MTT-S Int. Microw. Sympsoium Dig. (Cat. No.01CH37157)*, vol. 1, pp. 515–518, 2001.

[42] T. W. Kim, B. Kim, and K. Lee, "Highly Linear Receiver Front-End Adopting MOSFET Transconductance Linearization by Multiple Gated Transistors," *IEEE J. Solid-State Circuits*, vol. 39, no. 1, pp. 223–229, Jan. 2004.

[43] Yong-Sik Youn, Jae-Hong Chang, Kwang-Jin Koh, Young-Jae Lee, and Hyun-Kyu Yu, "A 2GHz 16dBm IIP3 low noise amplifier in 0.25μm CMOS technology," in *2003 IEEE International Solid-State Circuits Conference, 2003. Digest of Technical Papers. ISSCC.*, 2001, vol. 1, pp. 452–507.

[44] C. Xin and E. Sanchez-Sinencio, "A linearization technique for RF low noise amplifier," *Circuits Syst. 2004. ISCAS '04. Proc. 2004 Int. Symp.*, vol. 4, p. IV-313-16 Vol.4, 2004.

[45] H. M. Geddada, J. W. Park, and J. Silva-Martinez, "Robust derivative superposition method for linearising broadband LNAs," *Electron. Lett.*, vol. 45, no. 9, p. 435, 2009.

[46] V. Aparin, G. Brown, and L. E. Larson, “Linearization of CMOS LNA’s via optimum gate biasing,” in *2004 IEEE International Symposium on Circuits and Systems (IEEE Cat. No.04CH37512)*, 2004, vol. 4, p. IV-748-51.

[47] A. I. Mecwan and N. M. Devashrayee, “Linearity improvement of LNA using Derivative Superposition: Issues and challenges,” in *2017 7th International Conference on Cloud Computing, Data Science & Engineering - Confluence*, 2017, pp. 759–763.

[48] D. Im, I. Nam, H. T. Kim, and K. Lee, “A wideband CMOS Low noise amplifier employing noise and IM2 distortion cancellation for a digital TV tuner,” *IEEE J. Solid-State Circuits*, vol. 44, no. 3, pp. 686–698, 2009.

[49] T. W. Kim, B. Kim, Y. Cho, B. Kim, and K. Lee, “A 13 dB IIP3 improved low-power CMOS RF programmable gain amplifier using differential circuit transconductance linearization for various terrestrial mobile D-TV applications,” *IEEE Symp. VLSI Circuits, Dig. Tech. Pap.*, vol. 2005, no. 4, pp. 344–347, 2005.

[50] M. Parvizi and A. Nabavi, “Improved derivative superposition scheme for simultaneous second- and third-order distortion cancellation in LNAs,” *Electron. Lett.*, vol. 45, no. 25, p. 1323, 2009.

[51] V. Aparin and L. E. Larson, “Modified derivative superposition method for linearizing FET low-noise amplifiers,” *IEEE Trans. Microw. Theory Tech.*, vol. 53, no. 2, pp. 571–581, Feb. 2005.

[52] M. J. Zavarei, E. Kargaran, and H. Nabovati, “Design of high gain CMOS LNA

with improved linearity using modified derivative superposition," in *2011 18th IEEE International Conference on Electronics, Circuits, and Systems*, 2011, no. 4, pp. 322–325.

[53] S. Ganesan and E. Sanchez-Sinencio, "A highly linear low-noise amplifier," *IEEE Trans. Microw. Theory Tech.*, vol. 54, no. 12, pp. 4079–4085, 2006.

[54] W. Gao, Z. Chen, Z. Liu, W. Cui, and X. Gui, "A Highly Linear Low Noise Amplifier with Wide Range Derivative Superposition Method," *IEEE Microw. Wirel. Components Lett.*, vol. 25, no. 12, pp. 817–819, 2015.

[55] K.-Y. Kao, H.-Y. Lin, and K.-Y. Lin, "A 20 GHz power amplifier with IM3 distortion cancellation by load-split derivative superposition," in *2016 IEEE MTT-S International Microwave Symposium (IMS)*, 2016, vol. 2016–Augus, no. 1, pp. 1–4.

[56] S. Lou and H. C. Luong, "A Linearization Technique for RF Receiver Front-End Using Second-Order-Intermodulation Injection," *IEEE J. Solid-State Circuits*, vol. 43, no. 11, pp. 2404–2412, Nov. 2008.

[57] E. A. Keehr and A. Hajimiri, "Digitally-Assisted Linearization of Wideband Direct Conversion Receivers," in *2008 European Microwave Integrated Circuit Conference*, 2008, no. October, pp. 159–162.

[58] E. A. Keehr and A. Hajimiri, "Successive Regeneration and Adaptive Cancellation of Higher Order Intermodulation Products in RF Receivers," *IEEE Trans. Microw. Theory Tech.*, vol. 59, no. 5, pp. 1379–1396, May 2011.

[59] E. A. Keehr and A. Hajimiri, “A rail-to-rail input receiver employing successive regeneration and adaptive cancellation of intermodulation products,” *Dig. Pap. - IEEE Radio Freq. Integr. Circuits Symp.*, vol. 91125, pp. 47–50, 2010.

[60] M. Valkama, A. Shahed hagh ghadam, L. Anttila, and M. Renfors, “Advanced digital signal processing techniques for compensation of nonlinear distortion in wideband multicarrier radio receivers,” *IEEE Trans. Microw. Theory Tech.*, vol. 54, no. 6, pp. 2356–2366, Jun. 2006.

[61] a. Shahed hagh ghadam, M. Valkama, and M. Renfors, “Adaptive compensation of nonlinear distortion in multicarrier direct-conversion receivers,” *Proceedings. 2004 IEEE Radio Wirel. Conf. (IEEE Cat. No.04TH8746)*, pp. 35–38, 2004.

[62] E. Rebeiz, A. Shahed hagh ghadam, M. Valkama, and D. Cabric, “Suppressing RF Front-End Nonlinearities in Wideband Spectrum Sensing,” in *Proceedings of the 8th International Conference on Cognitive Radio Oriented Wireless Networks*, 2013.

[63] Q. Zou, M. Mikhemar, and A. H. Sayed, “Digital Compensation of Cross-Modulation Distortion in Software-Defined Radios,” *IEEE J. Sel. Top. Signal Process.*, vol. 3, no. 3, pp. 348–361, Jun. 2009.

[64] Qiyue Zou, M. Mikhemar, and A. H. Sayed, “Digital compensation of RF nonlinearities in software-defined radios,” in *2008 IEEE International Conference on Acoustics, Speech and Signal Processing*, 2008, pp. 2921–2924.

[65] S. S. Haykin, *Introduction to adaptive filters*. New York: Macmillan, 1984.

[66] J. A. Apolinário and S. L. Netto, “Introduction to adaptive filters,” *QRD-RLS Adapt. Filter.*, pp. 23–49, 2009.

[67] A. D. Poularikas and Z. M. Ramadan, *Adaptive Filtering Primer with MATLAB*. CRC Press, 2006.

[68] 3GPP, “LTE; Evolved Universal Terrestrial Radio Access (E-UTRA); Base Station (BS) Radio Transmission and Reception (Release 12),” vol. 0. 3GPP, 2017.